HyDrop v2: Scalable atlas construction for training sequence-to-function models

Hannah Dickmänken[1,2,3], Marta Wojno[5], Koen Theunis[1,2,3,4], Eren Can Ekşi[1,2,3], Lukas Mahieu[1,2,3,4], Valerie Christiaens[1,2,3,4], Niklas Kempynck[1,2,3], Florian V. De Rop[1,2,3,4], Natalie Roels[1,2,3], Katina I. Spanier[1,2,3], Roel Vandepoel[1,2,3], Gert Hulselmans[1,2,3,4], Suresh Poovathingal[1,4,5,#], Stein Aerts[1,2,3,4,#]

[1]Laboratory of Computational Biology, VIB Center for AI & Computational Biology, Leuven, Belgium.
[2]VIB-KU Leuven Center for Brain & Disease Research, Leuven, Belgium.
[3]Department of Human Genetics, KU Leuven, Leuven, Belgium.
[4]Aligning Science Across Parkinson's (ASAP) Collaborative Research Network, Chevy Chase, MD 20815, United States.
[5]VIB-KU Leuven Center for Brain & Disease Research, CBD Technologies, Single Cell & Microfluidics Expertise Unit, 3000 Leuven, Belgium.
[#]Shared corresponding authors. Email: suresh.poovathingal@kuleuven.be; stein.aerts@kuleuven.be

ORCID:

Gert Hulselmans: 0000-0003-2205-1899

Lukas Mahieu: 0009-0002-5085-6985

Stein Aerts: 0000-0002-8006-0315

Valerie Christiaens: 0000-0002-5024-8691

Koen Theunis: 0000-0002-0699-6676

Suresh Poovathingal: 0000-0002-3236-2255

Florian V. De Rop: 0000-0003-1883-871X

Hannah Dickmänken: 0000-0001-9707-9293

Summary

Deciphering cis-regulatory logic underlying cell type identity is a fundamental question in biology. Single-cell chromatin accessibility (scATAC-seq) data has enabled training of sequence-to-function deep learning models allowing decoding of enhancer logic and design of synthetic enhancers. Training such models requires large amounts of high-quality training data across species, organs, development, aging, and disease. To facilitate the cost-effective generation of large scATAC-seq atlases for model training, we developed a new version of the open-source microfluidic system HyDrop with increased sensitivity and scale: HyDrop v2. We generated HyDrop v2 atlases for the mouse cortex and *Drosophila* embryo development and compared them to atlases generated on commercial platforms. HyDrop v2 data integrates seamlessly with commercially available chromatin accessibility methods (10x Genomics). Differentially accessible regions and motif enrichment across cell types are equivalent between HyDrop-v2 and 10x atlases. Sequence-to-function models trained on either atlas are comparable as well in terms of enhancer predictions, sequence explainability, and transcription factor footprinting. By offering accessible data generation, enhancer models trained on HyDrop-v2 and mixed atlases can contribute to unraveling cell-type specific regulatory elements in health and disease.

Introduction

Cell type identity is encoded in the DNA sequence of *cis*-regulatory elements (CREs), such as enhancers[1]. By harboring binding sites for specific combinations of transcription factors (TFs), CREs orchestrate cell type-specific binding of TFs subsequently resulting in the expression of genes underlying the cell's identity. Thus, identifying CREs is a fundamental question in biology. Several experimental approaches are available to identify CREs and characterize their function[1,2]. Two commonly used approaches are (1) genome-wide profiling of TF binding, with assays such as Chromatin Immuno Precipitation sequencing (ChIP-seq)[3], Cleavage Under Target and Release Using Nuclease (CUT& RUN)[4], and Cleavage Under Targets and Tagmentation (CUT&Tag)[2]; and (2) genome-wide profiling of chromatin activity such as histone modifications and chromatin accessibility[1]. Measuring chromatin accessibility with Assay of Transposase Accessible Chromatin (ATAC) offers the most unbiased approach that can be performed in single cells (scATAC)[1].

Various tools are available to process scATAC data and identify cell-type-specific regulatory sequences[5–9] (i.e., differentially accessible regions, DARs). Combining scATAC with

gene expression information, regulatory regions can be linked to downstream target gene expression[10,11]. The rapid growth of machine learning, especially deep learning (DL) has opened new possibilities for accurately identifying specific TF binding sites (TFBS) within accessible regions. So-called sequence-to-function (S2F) models identify the nucleotide sequence patterns of regulatory elements in the non-coding genome with only scATAC information as training data[12–15] (for an in-depth review see De Winter et al. (2025)[16]).

However, the combination of the large demand for training data for DL models[12,15] and the sparse nature of scATAC data[1] results in a pressing need for large-scale data sets across species, genotypes, conditions, and developmental stages. Overcoming the challenge of limited scATAC enhancer data is possible by DL models using orthogonal data, as shown previously in work on the fly embryo[15]. This, however, requires additional information from large-scale *in vivo* experiments[15,17] that are not always readily available. In contrast, other groups have shown that training high-quality S2F models with merely scATAC data is possible in fly[14] and other (model) organisms[12–14]. Along the same line, a recent benchmarking study on various data modalities showed that training DL models on scATAC data only perform superior in predicting cell type-specific enhancers than non-DL methods or using other data modalities[12]. Importantly, the need for high-quality scATAC data with improved coverage is emphasized[12].

Most large-scale data sets focus on mouse data or cell lines, while less benchmarking is done on non-vertebrate model organisms, leading to an underrepresentation in the data landscape[12,13,18]. However, including complex tissues and organisms with more than a handful of cell types is essential as the computational identification of functional elements paves the way for fundamental biological questions on cell state regulation. Typically, experimental validation is costly and difficult to leverage on a large scale, especially for complex model organisms compared to cell lines. Enhancer prediction with S2F models enhances speed and accuracy towards wet lab experiments to eventually understand the grammar of cell-type specific regulatory sequences[12,14,15].

Over the recent years, various scATAC-seq methods have been developed primarily using either well-based combinatorial indexing strategies or microfluidics encapsulation technology (for an in-depth comparison, see De Rop et al., 2023[19]). In an earlier publication, we developed HyDrop, a microfluidics droplet technology based on deformable hydrogel indexing beads, which enables high-throughput profiling of both single-cell RNAseq and single nuclei ATAC seq[20]. Based on this work, we have improved several aspects of the technology to develop HyDrop-ATAC v2 (further addressed as HyDrop v2), which enables profiling of single-cell ATAC seq with higher detection sensitivity. Like commercial platforms for droplet-based scATAC-seq (e.g., 10X

93 Genomics Epi ATAC), HyDrop v2 uses a hydrogel-based single-cell indexing strategy with droplet
94 microfluidics. Alternative commercial platforms are based on microwell encapsulation of single
95 cells (BD Rhapsody) or use a well-based combinatorial indexing strategy (Scale Bioscience).
96 Overall, these commercial platforms are costly and/or require labor-intensive workflows that
97 hamper the generation of large-scale single-cell atlasing works of complex tissues[19]. Importantly,
98 beyond comparing the quality and costs of various scATAC techniques[19], no benchmarking has
99 been performed to assess the effect of different scATAC-seq techniques (e.g., commercial versus
100 custom platforms) on their capacity to train S2F models. Such a quantitative evaluation of scATAC
101 techniques becomes even more relevant in light of the facilitated use of DL for a broad research
102 audience[6,21,22].

103 To address the need for high-quality and low-cost scATAC data, we refined the open-
104 source microfluidic platform HyDrop. The next version, HyDrop v2, offers improved and consistent
105 data quality across multiple batches of bead production. In cutting-edge S2F models and
106 footprinting predictions in mouse cortex and fly embryo, HyDrop v2 data perform analogously to
107 commercial data. By offering highly accessible data generation with the open-source HyDrop v2,
108 we contribute to unraveling cell-type specific regulatory elements in health and disease with deep
109 learning.
110

111 Results

112 HyDrop bead chemistry optimization enables reproducible 113 fragment capturing

114 The bead barcoding chemistry in the previous version of HyDrop[20] was performed using
115 a 3-stage extension of DNA primers grafted onto polyacrylamide gel beads that were generated
116 using droplet microfluidics. This was achieved with 96 different barcoded DNA primers. Three-
117 stage barcoding with 96 barcoded DNA primers results in a barcode complexity of 96^3 = 884,736
118 barcodes. During each stage of this barcoding strategy, hydrogel beads were mixed with DNA
119 polymerase and a uniquely barcoded extension primer (Figure 1a). The extension of the grafted
120 primers in the beads was achieved by cyclic DNA polymerase extension. Before the next stage
121 of bead barcoding, the second strand was denatured, and beads were washed to remove the
122 second strand (Figure 1a). In the current version of HyDrop v2 bead production, the polymerase-
123 based cyclic extension of the barcoded primers was replaced by ligation of the barcoded primers.
124 Barcoded oligo cassettes are now ligated sequentially in a 3-stage barcoding process resulting in

125 same barcode complexity as the HyDrop v1 beads. Importantly, in the HyDrop v2 bead
126 production, there is no intermediate strand denaturation or cyclic addition of primers to beads
127 (Figure 1a), thereby enhancing the barcode stability (Figure 1d).

128 We compared the purity of individual barcodes per bead by single bead picking using a
129 micro-injection syringe followed by amplification and Sanger sequencing (Fig 1d, Fig S1f).
130 Compared to HyDrop v1, which showed higher barcode contamination across different barcodes,
131 all three ligated barcodes in the v2 beads are correctly individualized per bead.

132 An additional quality challenge that we faced with HyDrop v1 bead production was the
133 maintenance of stable bead quality, both in terms of the stability of the polyacrylamide gel bead
134 matrix as well as in the maintenance of the size of the gel beads during bead production. Both
135 factors are closely tied to the monomer composition of polyacrylamide chemistry. Earlier works
136 have demonstrated the structural stability of polyacrylamide chemistry is governed by the
137 monomer and crosslinker compositions[23]. Accordingly, a series of optimization cycles improving
138 the composition of total monomer concentration (%T) and crosslinker concentration (%C) (Figure
139 S1a) was performed. Based on different conditions we found 10% total monomer concentration
140 (T) and 2% crosslinker concentration to produce the most stable beads (Figure S1a). These
141 changes in bead generation were validated through multiple batches of beads that were produced
142 across seven independent bead production runs (Figure 1C, Figure S1d). The bead batches were
143 generated using an in-house fabricated microfluidics droplet generator as described earlier[20]. A
144 quality comparison of the hydrogel beads produced with commercial alternates (droplet generator
145 chips from Atrandi Biosciences) showed that the gel beads generated with the in-house fabricated
146 bead generator yield beads of superior quality (Figure S1d, e). This is primarily attributed to the
147 incompatibility of adding the N,N,N′,N′ -Tetramethylethylenediamine (TEMED), a polyacrylamide
148 polymerization catalyst with the Atrandi's droplet generation chips. TEMED was added post
149 droplet generation to the bead emulsion oil. Droplets generated using commercial chips
150 furthermore result in freezing artifacts from bead storage (Figure S1e).

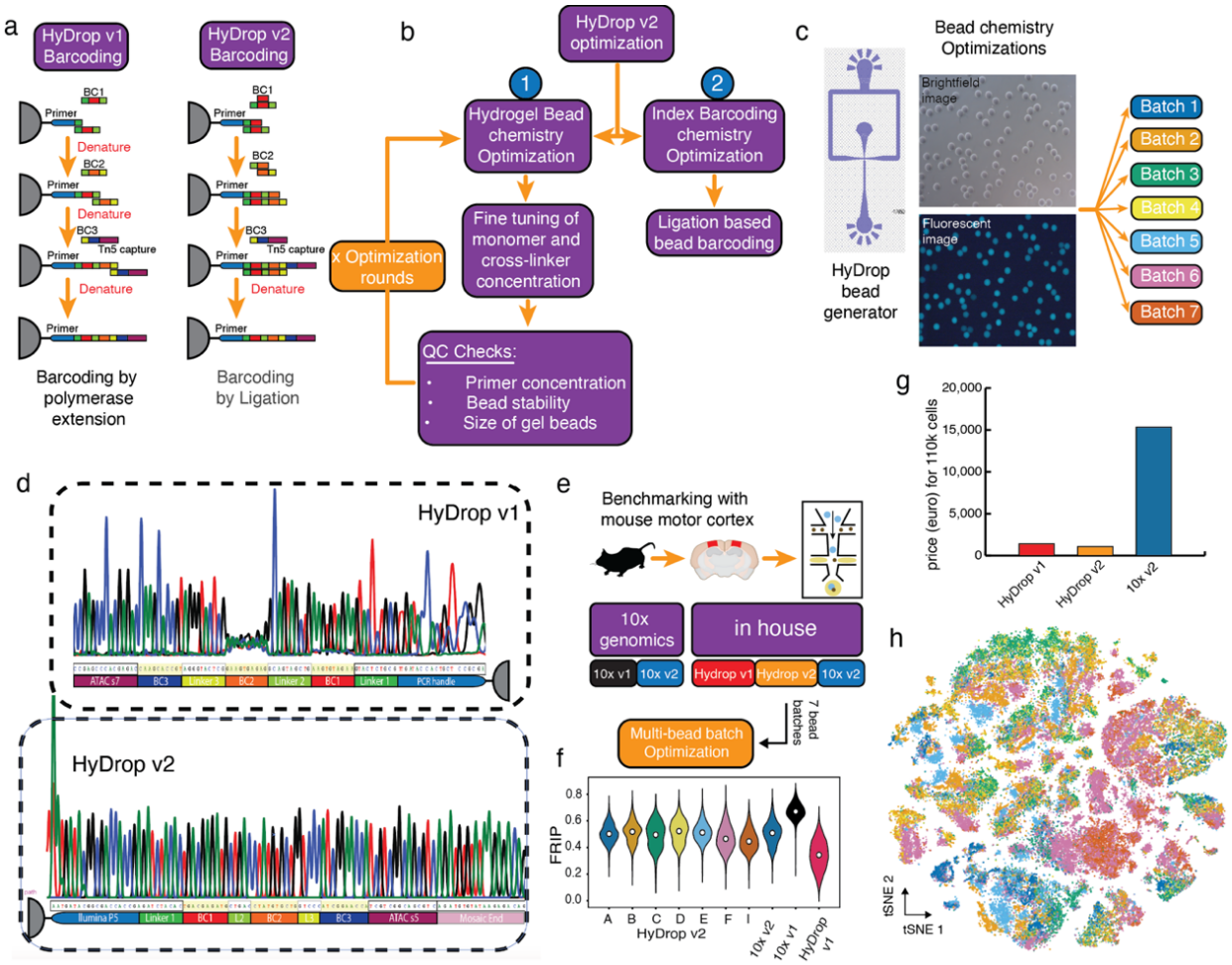

Fig. 1|Optimizations of HyDrop enable consistently high fragment capture. a, Comparison between bead barcoding chemistries of HyDrop v1 and v2. **b**, The HyDrop v1 protocol was optimized in two ways: (1) Bead chemistry was adjusted in several optimization rounds, and (2) the barcoding of the beads was changed from a cyclic polymerase extension to a linear ligation-based chemistry. **c**, The design of the microfluidic chip to generate HyDrop hydrogel beads (left), alongside the image of the polymerized hydrogel bead and fluorescence image of the bead labeled with complement of Tn5 fragment capture site. **d,** Sanger sequencing of an exemplary HyDrop v1 bead (top) showing impurity in barcode one and barcode two and a HyDrop v2 bead with pure barcode signals across all three barcodes. **e**, Mouse cortex data were partly downloaded from the official 10x genomics website and partly generated in-house. Overview of the sample generation: dissection of mouse motor cortex, tissue lysis followed by droplet encapsulation for cell barcoding. For HyDrop v1 only one bead batch was generated (data reused from De Rop et al., 2022) while for HyDrop v2 seven bead batches were generated (seen in c). **f**, FRIP of experiments pooled for seven different bead batches of HyDrop v2 compared to pooled 10x v2, 10x v1, and HyDrop v1 samples. The median is indicated per sample in white. **g,** Estimation of generation costs of 110k cells in euros excluding sequencing costs. HyDrop v1: 1,398.29 euros, HyDrop v2: 1,080.60 euros, 10x v2: 15,330.70 euros. **h**, *t*-distributed stochastic neighbor embedding (tSNE) of all 110,547 cells generated with HyDrop v2 (35 experiments) colored by bead batch (seen in c), no batch correction. Data points were randomly shuffled before plotting. QC: Quality control, FRIP: Fraction of reads in peaks.

We evaluated the changes in bead chemistry and generation by comparing commercial microfluidics platforms from 10x genomics to HyDrop v1 (one bead batch) and HyDrop v2 using mouse motor cortex tissue (Figure 1e). For HyDrop v2, seven independent bead batches were used, showing high data integrability without the need for batch correction (Figure 1h). The described changes in HyDrop v2 compared to HyDrop v1 result in improved performance in recovered unique fragments with an increase of 10.06%. Here, HyDrop v2 reaches, on average, 93.01% (M HyDrop v2=3.92, SD=0.38; M 10x v2=4.21, SD=0.27) of the unique number of fragments (log scaled) captured with 10x v2 (Figure S1b). Similarly, the fraction of reads found in peaks (FRIP, Figure 1f) in HyDrop v2 and the sequencing efficiency (Figure S2b) of Hydrop v2 nearly reached 10x genomics levels (M FRIP HyDrop v2=0.49, SD=0.09; M FRIP 10x v2=0.51, SD=0.09).

We generated an atlas of 110k cells covering the major cell types in the mouse motor cortex using the HyDrop v2 platform for 1,080.6 euros (excluding sequencing). Generating a data set of this size using HyDrop v1 would have cost 1,398.29 euros while using the current gold standard of scATAC sequencing (10x v2 chemistry) would result in a cost of approximately 15,330.70 euros (Figure 1g).

Here, we demonstrate that the improvements from HyDrop v1 to v2 chemistry result in reliable data generation of large-scale scATAC data sets in complex tissue covering various cell types. Additionally, we were able to reduce the costs of HyDrop even further while increasing the sequencing efficiency. Next, we perform an in-depth quality assessment of HyDrop v2 generated data across different model organisms, i.e., mouse and fly, for commonly used bioinformatic tools and novel deep learning applications.

HyDrop v2 captures the same cellular diversity in the mouse motor cortex as 10x v2

To evaluate the quality of the data generated with HyDrop v2, we generated scATAC-seq datasets on two complex tissues: the mouse cortex (Figure 1e) and the last four hours of *Drosophila melanogaster* embryo development (Figure 4a). To evaluate bead variability, we performed 35 experiments on frozen adult mouse cortex recovering a total of 110,547 cells after filtering (See Methods). For downstream analysis, the data integrates seamlessly with 10x (v1 and v2) and HyDrop v1 data (Figure S2a, c). With the combined data of 141,010 cells, we recover all major cell types of the mouse cortex (Figure 2a), annotated based on cell-type specific regions from two published data sets[12,24].

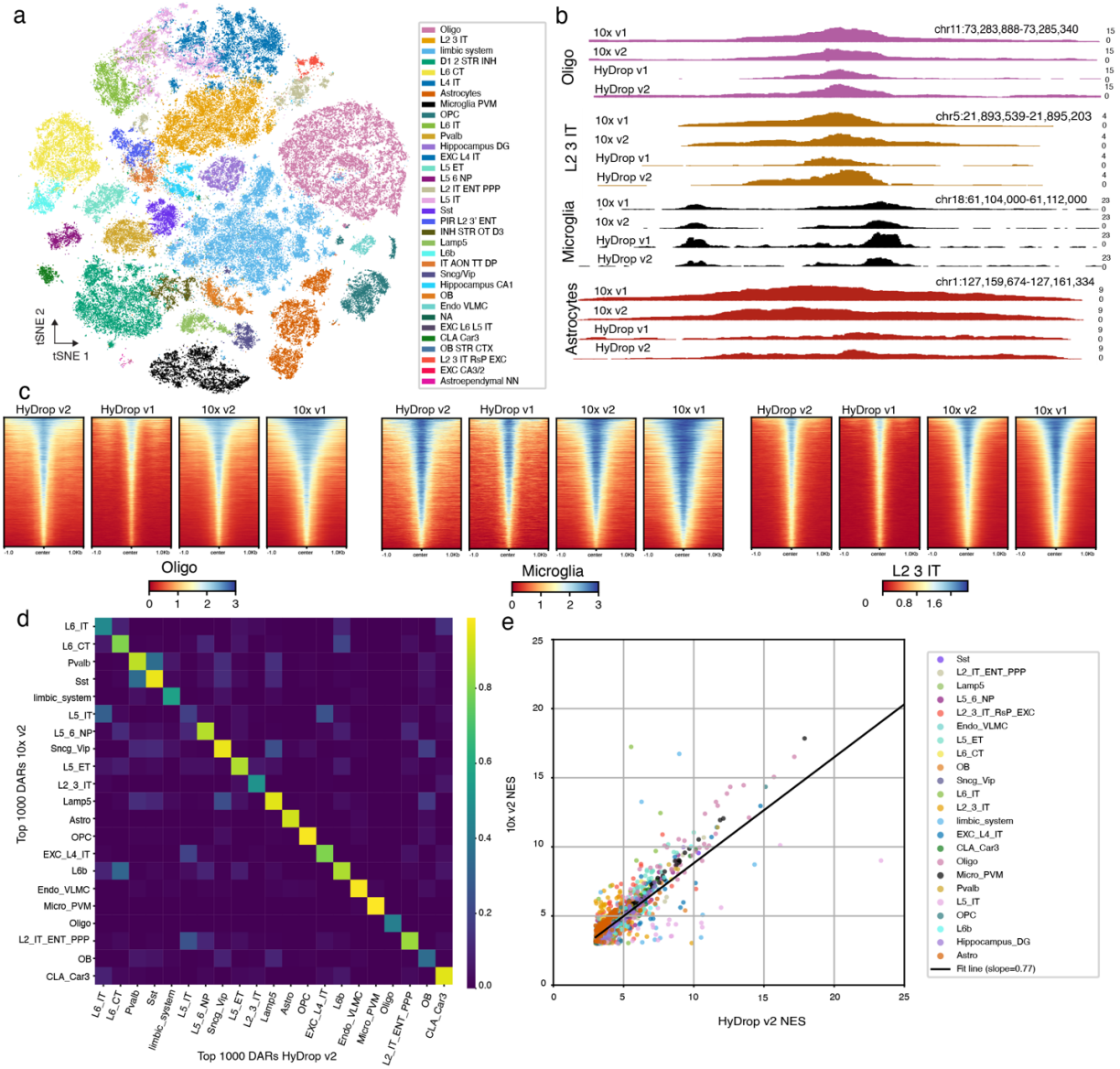

Fig. 2|Differential accessible regions in HyDrop v2 mouse cortex replicate regions identified by 10x. a, *t*-distributed stochastic neighbor embedding (tSNE) of all 141,010 cells across 44 experiments (2 experiments 10x v1 with a total of 10,177 cells, 2 experiments 10x v2 with a total of 13,123 cells, 5 experiments HyDrop v1 with a total of 7,163 cells, 35 experiments HyDrop v2 with a total of 110,547 cells) colored by cell type, batch corrected for the used technique. Data points were randomly shuffled before plotting. **b**, Genome tracks of cell-type specific DARs down sampled to the lowest cell number present for each technique, 985 cells in oligodendrocytes, 469 cells in L2 3 IT neurons, 509 cells in microglia, and 998 cells in astrocytes. The shown genome tracks are normalized for the fragment count. **c**, carrot plot showing the regions of accessible chromatin ±1 kb around the center of DARs (logFC ≥ 1.5), sorted by the highest (blue) to lowest (red) accessibility for oligodendrocytes, microglia, and L2 3 IT neurons across the four different techniques. **d**, Heatmap of percental overlap of top 1000 DARs per cell type of 10x v2 and HyDrop v2 data. **e**, Scatterplot of normalized enrichment score of cell-type-specific transcription motifs, dots represent a common motif between HyDrop v2 and 10x v2 data colored per cell type as shown in a. DAR: differentially accessible region, NES: normalized enrichment score.

To compare cell-type features in-depth, we calculated differentially accessible regions (DARs) of each cell type per technique (HyDrop v2, HyDrop v1, 10x v2, 10x v1). HyDrop v2 reveals a similar fragment coverage as 10x v1 and v2 data in example cell-type specific DARs (Figure 2b) as well as across all cell-type specific DARs (Figure 2c). Only focusing on the 1,000 highest scoring DARs, i.e., regions yielding important signature features of each cell type[19], reveals a high percental overlap between the regions recovered by HyDrop v2 and 10x v2 (Figure 2d): The mean overlap across cell types is 76.63% between 10x v2 and HyDrop v2 with a maximum of 98.8% recovering the same regions in microglia. Similarly, the 1,000 strongest DARs in HyDrop v1 show a mean overlap of 70.35% overlap with 10x v2 as well (Figure S2d).

Next, we evaluate the biological information covered in the cell-type specific DARs per technique using motif enrichment analysis (pyCisTarget[10]). The recovered motifs of 10x v2 and HyDrop v2 correlate highly on their normalized enrichment score (NES, r=.77) per cell type (Figure 2e), while HyDrop v1 performed slightly lower (NES r=.74, Figure S2e). A close-up of enrichment scores of exemplified cell types can be found in Figure S2f.

Sequence-to-function model identifies cell type-specific enhancers in the adult mouse cortex

Sequence-based deep learning models trained on scATAC data have been shown to identify cell-type specific sequence features in the genome[12,13]. Published models thus far have been trained on data generated by commercial platforms such as 10x genomics[12–14]. Here, we investigated whether scATAC-seq data generated by HyDrop v2 can be used to train performant S2F models. To this end, we first clustered all HyDrop v2 mouse cortex data, integrating seamlessly without batch correction (Figure 3a, 1h). Next, we trained S2F models using the CREsted package[22] on HyDrop v2 data predicting peak heights across cell types. To evaluate the model performance, we compared the HyDrop v2-based S2F model to a published model trained with 10x multi-ome data and which outperformed other S2F models earlier (see BICCN challenge[12] for details). When comparing the correlation of the prediction versus ground truth peak heights, both models closely predict the peak height as seen in their respective data sets (Figure S4a, b). The HyDrop v2 model outperforms the 10x model in the class-wise comparison on the full test set, while the 10x model scores slightly higher in the cell type-specific test set (Figure 3b) as classically seen for fine-tuned models[12,21]. In the region-wise comparison, HyDrop v2 closely follows the 10x model.

To investigate whether the HyDrop v2 model captures relevant biological information, we evaluate its peak height predictions and sequence explanations: Similar to previously published

247 models[13], the HyDrop v2-based model recovers the correct microglia TFBS in the FIRE enhancer
248 that replicate the findings of the 10x model (Figure 3c-d). Furthermore, the HyDrop v2 model can
249 correctly predict chromatin accessibility in an unseen locus such as the *Chsy3* gene (Pearson
250 correlation coefficient: 0.59), a marker gene of L6CT neurons (Figure 3e top). To investigate if the
251 HyDrop v2 model can identify enhancers across major mouse cortex cell types, we compared its
252 performance to a suite of enhancers earlier evaluated *in vivo*[25]. The HyDrop v2 model assigns the
253 validated enhancer sequences with an average precision (AP) of 0.70 to the correct cell types
254 (Figure 3f), while the optimized 10x model achieves an AP of 0.80. The prediction of enhancer
255 activity based on scATAC information is comparable between HyDrop v2 and 10x data (Figure
256 3f, AP: 0.91-0.93). A similar observation is made when looking at the separate enhancers per cell
257 type (Figure S3).
258 To further investigate the sequence explainability of each model for cell type-specific
259 enhancers, we performed de novo motif discovery using *tfmodisco lite*[26] through the CREsted
260 package[22]. Per trained model (10x vs HyDrop v2), we identified enriched patterns, alongside their
261 individual instances (called seqlets). For the highest and lowest scoring patterns with a
262 contribution score cut-off 4.25, we find the same patterns in cell types in 10x and HyDrop v2 data
263 for astrocytes and microglia (Figure 3h, i) just as for several neuronal cell types (Figure S4g-j).
264 S2F models trained on commercial scATAC data have been shown to accurately identify
265 cell-type specific regions and predict TF binding sites[13]. Here, we show that a model trained on
266 non-commercial data generated with our open-source HyDrop v2 protocol achieves similar
267 performance to an optimized and fine-tuned 10x model and, importantly, can recover cell type-
268 specific regions and TF-binding sites. To investigate whether the slight difference in performance
269 can be attributed to model variability or a difference in training data quality, we trained two models
270 with 10-fold cross-validation on 10x v2 and HyDrop v2 of the *Drosophila* embryo generated with
271 the same library preparation protocol, data processing, and model architecture (see below).

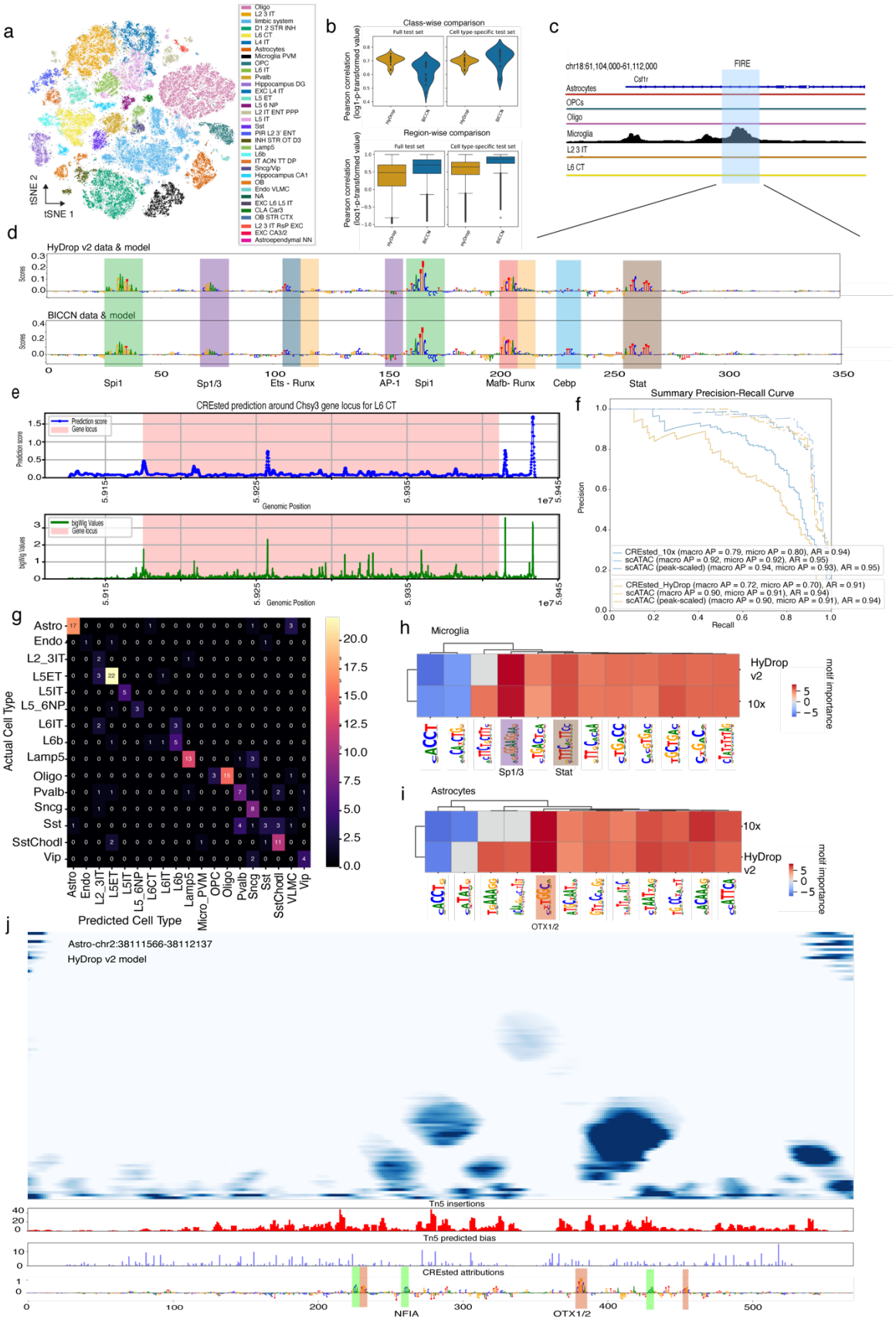
a
tSNE 1
tSNE 2
b
Class-wise comparison
Full test set
Cell type-specific test set
Pearson correlation (log1-p-transformed value)
Region-wise comparison
c
chr18:61,104,000-61,112,000
FIRE
Csf1r
Astrocytes
OPCs
Oligo
Microglia
L2 3 IT
L6 CT
d
HyDrop v2 data & model
BICCN data & model
Scores
Spi1
Sp1/3
Ets - Runx
AP-1
Mafb- Runx
Cebp
Stat
e
CREsted prediction around Chsy3 gene locus for L6 CT
Prediction score
Gene locus
bigWig Values
Genomic Position
f
Summary Precision-Recall Curve
Precision
Recall
CREsted_10x (macro AP = 0.79, micro AP = 0.80), AR = 0.94)
scATAC (macro AP = 0.92, micro AP = 0.92), AR = 0.95)
scATAC (peak-scaled) (macro AP = 0.94, micro AP = 0.93), AR = 0.95)
CREsted_HyDrop (macro AP = 0.72, micro AP = 0.70), AR = 0.91)
scATAC (macro AP = 0.90, micro AP = 0.91), AR = 0.94)
scATAC (peak-scaled) (macro AP = 0.90, micro AP = 0.91), AR = 0.94)
g
Actual Cell Type
Predicted Cell Type
Astro
Endo
L2_3IT
L5ET
L5IT
L5_6NP
L6CT
L6IT
L6b
Lamp5
Micro_PVM
OPC
Oligo
Pvalb
Sncg
Sst
SstChodl
VLMC
Vip
h
Microglia
HyDrop v2
10x
motif importance
Sp1/3
Stat
i
Astrocytes
OTX1/2
j
Astro-chr2:38111566-38112137
HyDrop v2 model
Tn5 insertions
Tn5 predicted bias
CREsted attributions
NFIA
OTX1/2

Fig. 3|Hydrop v2 produces comparable training data for cutting-edge deep learning tools as public 10x data set. a, *t*-distributed stochastic neighbor embedding (tSNE) of all 110,547 cells generated with HyDrop v2 (35 experiments) colored by cell type, no batch correction. Data points were randomly shuffled before plotting. **b,** Model comparison of sequence models trained on HyDrop v2 data (orange) and the BICCN (10x) public data set (i.e., 10x multi-ome data in blue). The accuracy of the predictions evaluated based on the ground truth of region accessibility is compared on class-wise (top) and region-wise level (bottom) for both the full test set in the data and cell type-specific test sets. **c**, Genome tracks of cell-type specific chromatin accessibility of the FIRE enhancer (mm10 chr18:61108475-61108975), regulating Csf1r expression in microglia. **d**, Nucleotide contribution score of the FIRE enhancer from a sequence model trained on HyDrop v2 data (top) and a model trained on 10x data. Previously described TF binding sites are highlighted for the corresponding TF. **e,** Prediction by the HyDrop v2 sequence model on HyDrop v2 data of chromatin accessibility for L6 CT (top) around the Chsy3 gene locus compared to actual chromatin accessibility plotted from the corresponding bigwig file (bottom). **f**, Specificity prediction for *in vivo* enhancer activity of validated mouse cortex enhancers by Ben-Simon et al. (2024) shown for the HyDrop v2 and BICCN (10x-based) model. **g,** Heatmap of enhancer indicated by Ben-Simon et al. (2024) identified as cell-type specific enhancer of the corresponding cell type by the HyDrop v2 model. **h**, **i,** Evaluation of motif importance scores of highly relevant regions for cell type identity indicated by the BICCN (10x) data-based model and HyDrop v2 data-based model for microglia (**h**) and astrocytes (**i**) with motifs shown in d and j, respectively, are identified and highlighted. **j,** Multiscale footprint of the region (mm10 chr2:38111566-38112137) of HyDrop v2 data only. Bottom tracks show Tn5 insertion, the predicted Tn5 bias and the nucleotide contribution scores based on the HyDrop v2 sequence model. Previously described TF binding sites are highlighted for the corresponding TF.

Cellular diversity in Drosophila embryos is captured comparably with HyDrop v2 and 10x v2

Apart from the mouse cortex samples, we compared the optimized HyDrop v2 protocol on another complex biological system, the developing fruit fly. *Drosophila melanogaste*r is widely used for developmental research[27] but is rarely included in larger benchmarking studies of scATAC techniques[19,20]. Here, we compare in-house generated HyDrop v2 and 10x v2-based data of the last four hours of *Drosophila* embryo development (stage 17)[27]. Additionally, we compare the quality of these two microfluidic platforms to public data from the *Drosophila* embryo of the same age[27] generated with sciATAC-seq3, a plate-based assay using combinatorial indexing[28] (Figure 4a). We generated a new embryo atlas with 10x v2 and HyDrop v2, with a total of 607,340 cells (HyDrop v2: 340,604 cells, 10x v2: 266,736 cells, Figure 4b). We annotated this new atlas based on the region accessibility of DARs of the public embryo atlas[27] combined with annotated activity patterns of *in vivo* tested enhancers[17]. HyDrop v2 reveals a similar fragment coverage as 10x v2 data in, cell-type specific DARs (Figure 4d top, S5d) as well as across all cell-type specific DARs (Figure 4e left, S5e). sci-ATAC data exhibits a wider range of accessibility across regions compared to 10x v2 and HyDrop v2 data (Figure 4d, e and S5d,e). However, when

310 focusing on the cut sites of Tn5 (Figure 4d bottom, S5d), sciATAC resembles the Tn5 insertion
311 profile observed in 10x v2 and HyDrop v2 data, yielding a more distinct identification of accessible
312 region across all cell-type specific DARs (Figure 43 right, S5e). Possibly due to the larger fragment
313 size covering wider regions of the genome (Figure 4d, S5c-d), sciATAC has a significantly higher
314 fraction of reads in peaks (FRIP) than HyDrop v2 and 10x v2 (Figure 4c left, H(2) = 37,728,
315 p<.001) while both 10x v2 and HyDrop v2 score higher on TSS enrichment (Figure 4c middle,
316 H(2) = 172,030, p<.001) and the number of unique fragments per 12k reads per cell (Figure 4c
317 left, H(2) = 48,846, p<.001). The in-house generated data was downsampled to 12k reads per
318 cell to not overestimate the read compared to sciATAC[27]. Similar to mouse HyDrop v2 data, the
319 slightly higher ability to recover unique fragments of 10x v2 versus HyDrop v2 is reflected by its
320 more efficient sequencing at the same depth (Figure S5g). When investigating the depth of
321 biological information, we found that the most important 1,000 DARs identified by HyDrop v2 or
322 10x v2 overlap with a mean of 80.57% across cell types (Figure 4f), just as in the mouse cortex
323 data. When performing motif enrichment analysis[10], we observed a strong correlation (r=.95) of
324 the enrichment score of individual enriched motifs between 10x v2 and HyDrop v2 data (Figure
325 4g) and, to a slightly lesser extent, in 10x v2 and sciATAC (Figure S5h, r=.92).
326 Just as for mouse cortex scATAC, we show that HyDrop v2 offers a comparable alternative
327 to 10x v2-based data in the developing fruit fly. Overall, HyDrop v2 *Drosophila* embryo data quality
328 has a slightly lower sensitivity *per cell* compared to 10x v2 but due to the low cost, larger atlases
329 can be constructed and at the atlas level, the quality of detecting DARs and enriched motifs
330 become equivalent.

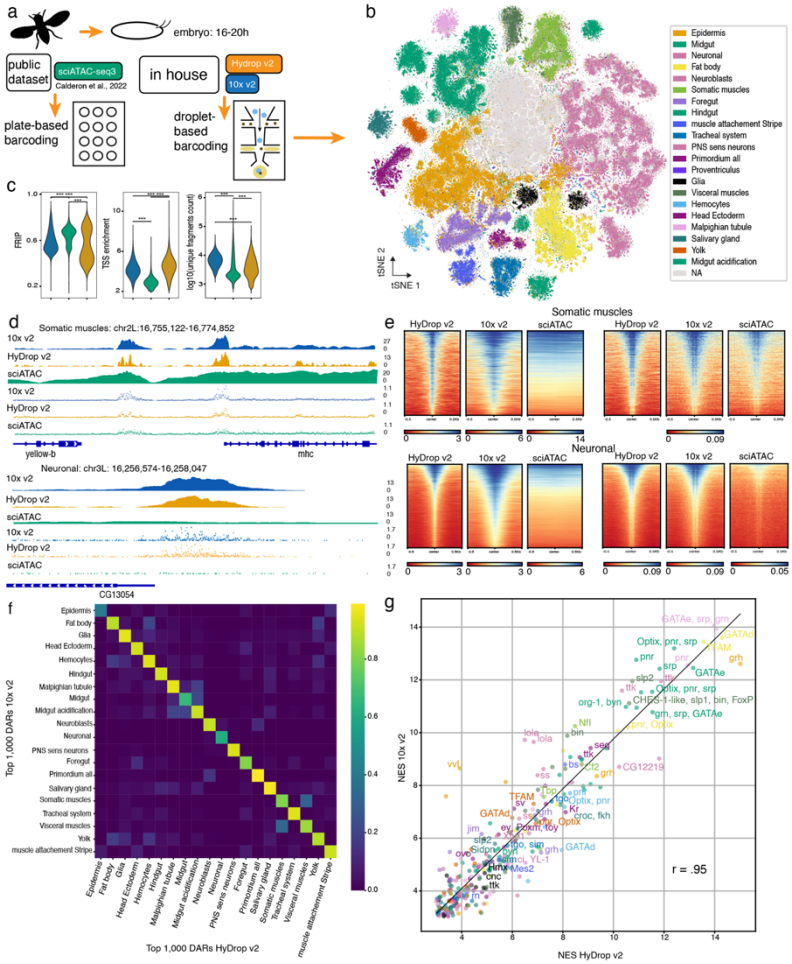

Fig. 4|HyDrop v2 captures cellular diversity in developing Drosophila melanogaster. a, Overview of study design. Drosophila melanogaster embryos were collected 16-20h after egg laying. In-house experiments were performed with 10x v2 chemistry on the 10x Chromium device, while HyDrop v2 beads were used for the open-source data generation. sciATAC-seq3 data (fragment files for the plate-based essay) were retrieved from Calderon et al., (2022). **b**, *t*-distributed stochastic neighbor embedding (tSNE) of all 607,340 cells generated with HyDrop v2 (340,604, 18 experiments) and 10x v2 (266,736 cells, 5 experiments) colored by cell type, batch correction according to wet lab protocol used to generate data. Data points were randomly shuffled before plotting. **c,** Violin plots of quality measurements (TSS enrichment, FRIP, log fragment counts) compared between 10x v2, sciATAC-seq3, and HyDrop v2 data**. d,** Genome tracks (upper) and cut site insertion of Tn5 (lower) of cell-type specific DARs down sampled to the smallest count present for each technique, 1,861 cells in neuronal cells and 8,916 cells in somatic muscle cells. The shown genome tracks are normalized for the fragment count. **e**, Carrot plot showing the regions of accessible chromatin ±0.5 kb around the center of DARs sorted by the highest (blue) to lowest (red) accessibility for neuronal cells and somatic muscle cells in 10x v2, HyDrop v2, and sciATAC data. DARs are calculated on fragment coverage (left) and Tn5 cut sites (right) for each technique. **f**, Heatmap of percental overlap of top 1,000 DARs per cell type of 10x v2 and HyDrop v2 data. **g,** Scatterplot of normalized enrichment score of cell-type-specific transcription motifs, dots represent a common motif between HyDrop v2 and 10x v2 data colored per cell type as shown in a, the labels are shown for the top three motifs per cell type. DAR: differentially accessible region, TSS: Transcription start side, FRIP: fraction of reads in peaks.

Essential regions in validated Drosophila enhancer recovered by Hydrop-v2 based deep learning model

Apart from investigating data quality in terms of the common bioinformatics analyses, e.g., DARs, and motif enrichment analysis, we trained separate S2F sequence models on the *Drosophila* embryo data for 10x v2 and HyDrop v2 (Figure 5a). Again, the fly models were trained using the CREsted package, although for fly we applied additional filtering on the standardized peak heights (see Methods). Both, the model based on 10x v2 and the model based on HyDrop v2 score identical on region and class-wise prediction of databased accessibility (Figure S6a-c).

To evaluate the ability of our S2F models to capture biologically relevant information, we made use of validated enhancers[17] analogous to the evaluation of the mouse models. Kvon et al. (2014) characterized 3,557 developmental enhancers *in vivo* according to tissue specificity of enhancer activity. This valuable enhancer database contains 2,693 enhancers assayed in stages 15-16 of which 80 are highly active with a specificity of maximally five tissues[17]. As the characterized enhancers have a length of approximately 2kb (Figure 5b), we scanned the regions with a sliding window of 500 bp (Figure 5c) in a 10 bp shift to determine the region that is the most relevant for the enhancer activity in the respective tissues in (Table S1) according to our S2F models. Both HyDrop v2 and 10x v2, as well as their respective 10-fold cross-validation models (shown as confidence intervals), identify the same 500 bp regions as primarily accessible across 2kb enhancers (Figure 5d, S6d). Enhancer VT3067, mainly active in the ventral nerve cord (VNC, Figure 5e), is predicted to be accessible in neuroblasts (NBs, Figure 5f), linking activity to enhancer accessibility of the 500 bp window with the highest predictive value. Also, in other tissues, the observed *in vivo* activity[17] corresponds to the predicted accessibility in the matching cell type based on the highest scoring 500 bp window of the respective enhancer using the HyDrop v2 model (Figure S6f,h for midgut cells, S6j,l for foregut cells, S6n,p for epidermis).

In the developing *Drosophila*, NBs type 1 and 2 are found in the VNC giving rise to neurons and glia[29] with the first wave of neurogenesis at the end of embryo development[30]. The nucleotide contribution scores of both HyDrop v2 and 10x v2, indeed predict motifs of NB-specific TFs such as *klumpfuß* (*klu*)[31] and *tramktrack* (*ttk*)[29] (Figure 5g). Interestingly, performing *tfmodisco lite* identifies the *ttk* motif (TCCT, ACCC) in NB and neurons but not glia. This is in line with well-established findings of *ttk* repressing glial fate in differentiating NBs[29]. Notably, the observed TF-motifs such as *ttk* or aspecific CA repeats match the reported motifs by the earlier central nervous system (CNS) S2F model trained on a combination of sciATAC data and enhancer activity data [15], as NBs occur in the CNS of the developing *Drosophila* embryo[29]. Comparing somatic and

visceral muscle cells, we observe different motifs with, e.g., *dorsal* only being predicted in somatic muscle cells (Figure 5j). The ability to identify different motifs in closely related tissues underlines the power of HyDrop v2 S2F to models to capture biological relevance.

The authors of the previously published *Drosophila* embryo S2F models designed synthetic enhancers for five tissues (CNS, brain, muscle, epidermis, and gut) using one model per tissue as a guiding oracle[15]. Per tissue, the activity of eight enhances was validated *in vivo*[15]. To compare our HyDrop v2 and 10x v2-based models with the sci-ATAC-based models, we evaluated the synthetic sequences designed by de Almeida et al. (2023). Due to the higher resolution in the annotation of our data and a model design that includes all cell types, we could specify that synthetic enhancer 1[15], which is designed for muscle cells, is indeed specific for somatic muscles across the *Drosophila* embryo (Figure 5k). Additionally, the HyDrop v2 model recovers all motifs indicated by the sciATAC model, while the 10x model is missing one *Trithorax-like* (*trl*) motif (Figure 5i). Similarly, nucleotide contribution scores of synthetic epidermis enhancer 6 (Figure 5h, S7c) show the typical *grainyhead* (*grh*) motif; a TF essential to epithelial cell fate[32]. The multi-class set of our HyDrop v2 S2F model allows for scoring synthetic enhancer activity across tissues. Synthetic enhancer 8, originally designed for epithelial cells, is mainly predicted to be accessible in glial cells based on our model (Figure S7d). Evaluating the nucleotide contribution indicates *repo* motif instances, being indicative for glia[29], in both 10x v2 and HyDrop v2 data. The mix of motifs from different tissues in this enhancer identified by our models might explain the lower predicted activity in the original sciATAC-based model[15].

Notably, not all of the previously designed synthetic enhancers showed (matching) *in vivo* activity[15]. Especially the brain and gut enhancer design is mentioned to be cumbersome. While the brain is a highly heterogeneous tissue itself, the gut poses the difficulty of being developed from the ectoderm (foregut and hindgut) and endoderm (midgut)[33], making a targeted synthetic enhancer design possibly less straightforward compared to tissues with one developmental origin. By including a large variety of tissues into one single model, we find that the synthetic enhancers that are not specifically active in the target tissue[15] (generally speaking, the gut) are also predicted to be active in other tissues outside the gut (Figure S73). This offers a possible explanation for the lack of specificity observed by de Almeida et al. (2023).

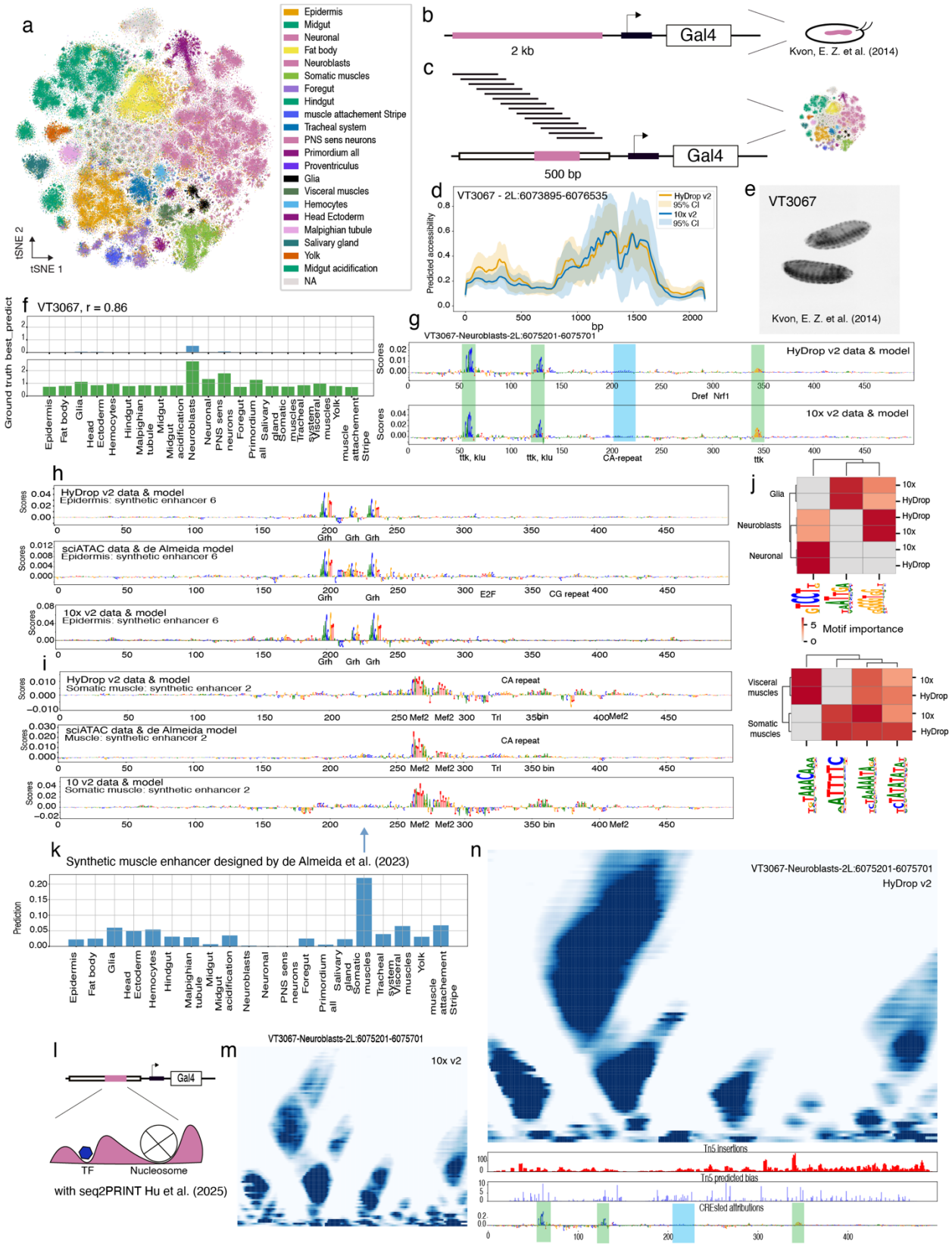
a
tSNE 2
tSNE 1
Epidermis
Midgut
Neuronal
Fat body
Neuroblasts
Somatic muscles
Foregut
Hindgut
muscle attachement Stripe
Tracheal system
PNS sens neurons
Primordium all
Proventriculus
Glia
Visceral muscles
Hemocytes
Head Ectoderm
Malpighian tubule
Salivary gland
Yolk
Midgut acidification
NA
b
2 kb
Gal4
Kvon, E. Z. et al. (2014)
c
500 bp
Gal4
d
VT3067 - 2L:6073895-6076535
HyDrop v2
95% CI
10x v2
95% CI
Predicted accessibility
bp
e
VT3067
Kvon, E. Z. et al. (2014)
f
VT3067, r = 0.86
Ground truth best_predict
g
VT3067-Neuroblasts-2L:6075201-6075701
HyDrop v2 data & model
10x v2 data & model
Scores
Dref Nrf1
ttk, klu
CA-repeat
ttk
h
HyDrop v2 data & model
Epidermis: synthetic enhancer 6
sciATAC data & de Almeida model
Epidermis: synthetic enhancer 6
10x v2 data & model
Epidermis: synthetic enhancer 6
Grh
E2F
CG repeat
j
Glia
Neuroblasts
Neuronal
10x
HyDrop
Motif importance
i
HyDrop v2 data & model
Somatic muscle: synthetic enhancer 2
sciATAC data & de Almeida model
Muscle: synthetic enhancer 2
10 v2 data & model
Somatic muscle: synthetic enhancer 2
CA repeat
Mef2
Trl
bin
Visceral muscles
Somatic muscles
k
Synthetic muscle enhancer designed by de Almeida et al. (2023)
Prediction
n
VT3067-Neuroblasts-2L:6075201-6075701
HyDrop v2
Tn5 insertions
Tn5 predicted bias
CREsled attributions
l
Gal4
TF
Nucleosome
with seq2PRINT Hu et al. (2025)
m
VT3067-Neuroblasts-2L:6075201-6075701
10x v2

414

Fig. 5|HyDrop v2 data enables training of sequence-based Deep Learning model to uncover cell-type specific transcription factor motifs and footprints in Drosophila embryo. a, *t*-distributed stochastic neighbor embedding (tSNE) of 340,604 cells (18 experiments) HyDrop v2 colored by cell type, no batch correction is applied. Data points were randomly shuffled before plotting. **b,** VDRC library of transgenic flies with ~2kb enhancers (pink) upstream of minimal promotor and Gal4 reporter. 2,693 enhancers stage 15-16 evaluated *in vivo* by Kvon et al. (2014). **c,** Scanning of ~2kb enhancers with sliding window (10bp shift) of 500 bp evaluated on cell types seen in a. **d,** Predicted accessibility of 500 bp windows of VT3067 enhancer from VDRC library. Both, the predictions based on the HyDrop v2 and 10x v2 data are shown with confidence intervals of 10-fold replicate models. **e,** *In situ* hybridization of VT3067-Gal4 reporter embryos stage 15 with antisense Gal4 probe by Kvon et al. (2014). **f,** Prediction (top) versus ground truth (bottom) of 500bp region within 2kb long VDRC enhancer VT3067 active in neuroblasts. **g,** Nucleotide contribution score of the 500 bp within VT3067 enhancers (VDRC fly line) trained on HyDrop v2 data (top) and 10x v2 data (bottom). Previously described TF binding sites are highlighted for the corresponding TF. **h,** Nucleotide contribution score of the 500 bp of synthetic enhancer designed to be active in epithelial cells based on sciATAC data by de Almeida et al. (2023): HyDrop v2 and 10x v2 model predictions shown for epithelial cells versus predictions by the original model for somatic muscle cells data. Previously described TF binding sites are marked for the corresponding TF. **i,** Nucleotide contribution score of the 500 bp of synthetic enhancer designed to be active in muscle cells based on sciATAC data by de Almeida et al. (2023): HyDrop v2 model predictions shown for somatic muscle cells (top) versus predictions by the original model for general muscle cells data (bottom). Previously described TF binding sites are highlighted for the corresponding TF. **j,** Evaluation of motif importance scores of highly relevant regions for cell type identity indicated by the 10x v2 data-based model and HyDrop v2 data-based model for neurons, glia, neuroblasts, and visceral muscles compared to somatic muscles. An importance threshold of 5 was handled. **k,** Prediction of tissue accessibility of synthetic enhancer designed for muscle cells in 10-12h embryos. Enhancers were designed by de Almeida et al. (2023) and scored with the HyDrop v2 model. Accessibility is specifically predicted for somatic muscle cells in the HyDrop v2 data. **l,** Schematic overview of possible footprinting in selected 500 bp region of VDRC library enhancers. Footprinting is performed with seq2PRINT suit by Hu et al. (2025). **m,** Multiscale footprint of 500bp region in VT3067 in 10x v2 data. **n,** Multiscale footprint of 500bp region in VT3067 in HyDrop v2 data only. The bottom track shows Tn5 insertion, the predicted Tn5 bias, and the nucleotide contribution scores based on the HyDrop v2 sequence model. Previously described TF binding sites are highlighted for the corresponding TF. VDRC: Vienna Drosophila Resource Center

Overall, we show that HyDrop v2 produces data of high quality that can be used to train multi-class S2F models, revealing biologically relevant features that closely resemble findings from 10x S2F models. Possible variations between models can be attributed to model variability, as shown in the 10-fold cross-validation (Figure 5d). Additionally, in *Drosophila*, we identified the core 500 bp of *in vivo* validated enhancers and replicated the findings of synthetic enhancer design in the *Drosophila* embryo.

HyDrop v2 matches transcription factor footprints found in 10x data in validated mouse and *Drosophila* enhancers

Next, we benchmarked the performance of HyDrop v2 data against 10x data to predict TF footprints. To this end, we applied the recently developed seq2PRINT framework[34]. seq2PRINT uncovers footprints of DNA-protein interaction in scATAC and bulk ATAC data after correcting Tn5 bias with a convolutional neural network[34]. The use of a species-specific Tn5 bias model permits the evaluation of possible footprints of nucleosomes and smaller proteins, such as transcription factors, in *Drosophila* and mouse cortex data. We first investigated whether the Tn5 bias differs between HyDrop v2 and 10x data, by comparing the Tn5 cut sites across techniques, species, and cell types. Tn5 cut sites obtained by HyDrop and 10x per cell type appear uniformly flanking the center of the peak in the accessible regions in mouse (Figure S4k-m) and fly (Figure 4d, S5e). The footprint around the center of the peak reflects the seq2PRINT-given Tn5 bias consistently in each cell type (Figure S4k-m, S5f). Interestingly, the footprint (the double vertical line) tends to be more visible in *Drosophila* due to the higher Tn5 concentration - relative to the small genome of 180 Mb[35] - resulting in smaller fragments. Consequently, performing the library preparation with the same Tn5 concentration as in mouse (see Methods) results in a higher insertion ratio of Tn5, leading to shorter fragments in *Drosophila* (Figure S5c) compared to mouse (Figure S1g). Importantly, just as in mouse, the Tn5 bias does not differ between HyDrop v2 and 10x v2 in *Drosophila* samples.

After correcting for possible Tn5 bias, we apply seq2PRINT in mouse (HyDrop v2 data and 10x-multi-ome data[12] from the 10x mouse model) and *Drosophila* (HyDrop v2 data and in-house 10x v2 data). In mouse, seq2PRINT identifies possible TF footprints that align with the predicted motifs based on the S2F model in the *in vivo* validated enhancers in astrocytes (Figure 3j, S4e), L5 ET neurons (Figure S4c,d), and oligodendrocytes (Figure 4f). Larger footprints indicating nucleosome binding coincide with the depletion of motifs. Importantly, the predicted footprints in HyDrop v2 data largely correspond to 10x data-observed footprints.

In the *Drosophila* embryo, we focused on the 500 bp window with the highest prediction score of the *in vivo* validated enhancers. We observed possible footprints coinciding with motif locations predicted by the S2F models that match between HyDrop v2 and 10x v2-based seq2PRINT predictions for NBs (Figure 5m,n), midgut cells (Figure S6e,g), foregut cells (Figure S6i,k), and epidermis cells (Figure S6m,o).

In conclusion, the improvements from HyDrop v1 to v2 chemistry result in reliable data generation of large-scale scATAC data sets in complex tissue covering various cell types. Our

484 results show that HyDrop v2 data enables building large-scale atlases with similar resolution to
485 the gold standard commercial microfluidic platform in mouse and fly achieving comparable
486 findings in commonly used bioinformatic applications and novel deep learning tools.
487

488 Discussion

489 Identifying cell-type-specific regulatory sequences from scATAC-seq data has become a
490 driving force behind the unraveling of gene regulatory networks but the cost-effective generation
491 of comprehensive scATAC-seq atlases is often a bottleneck. While S2F models offer powerful
492 ways to identify CREs such as enhancers, their performance strongly depends on the quality and
493 modality of training data[12]. Currently, scATAC-seq data acts as the gold standard for S2F model
494 training[12,13,21,34]. To address the need for accessible, high-quality, and cost-efficient scATAC-seq
495 data generation, we improved upon our previously established open-source microfluidic platform
496 HyDrop (now HyDrop v2), enabling consistent generation of large-scale data for improved DL-
497 based enhancer identification.
498 First, we generated large atlases of the mouse motor cortex with 110k high-quality cells
499 and the developing embryo of age 16-20h after egg laying of *Drosophila melanogaster* with 340k
500 cells using the novel HyDrop v2 platform. The costs of generating the library of, for example, the
501 mouse cortex across 35 experimental "runs" accumulate to merely 1,080.60 euros compared to
502 an equivalent of 10x v2-based library preparation for 15,330.70 euros, excluding the sequencing
503 cost. With the improved workflow, a single trained technician can perform 16 HyDrop v2 runs in
504 1.5 days. Thus, generating >100k cells of mouse cortex library becomes feasible within a few
505 days, making large-scale data generation with HyDrop v2 possible at low cost and scale.
506 After library preparation, the batches are sequenced to a desired read depth per cell. Here,
507 HyDrop v2 libraries reach a comparable number of unique fragments per cell to 10x data but
508 require a higher sequencing depth (i.e., having a lower sequencing efficiency). Nevertheless, we
509 found that the differentially accessible regions per cell type captured in the HyDrop v2 atlases are
510 equivalent to the 10x-recovered regions in mouse and fly, even after equilibrating for sequencing
511 depth (i.e., raw number of reads per cell). This confirms earlier findings showing that the number
512 of DARs does not depend on sequencing depth[19]. HyDrop v2 libraries already deliver comparable
513 quality to 10x data at a sequencing depth of 36kRPC for mouse and 12kRPC for the *Drosophila*
514 embryo. HyDrop v2 data integrates seamlessly with data from other microfluidics-based
515 platforms, and the assay can therefore also be used for protocol optimization before investing in

516 a major experiment. Eventually, data generated with different droplet-based platforms can be
517 combined for large-scale atlases across species.

518 Next, we evaluated the performance of HyDrop v2-based atlases in two deep learning
519 tools: ready-to-use S2F modeling[22] and seq2PRINT[34]. As the mouse cortex is well represented in
520 available S2F models, we chose a published 10x-based model[12] to compare our default HyDrop
521 v2 model. Across the major mouse cortex cell types, the HyDrop v2 model learned relevant
522 sequence features and identified candidate motifs comparable to the 10x-based model. In
523 predicting the activity of *in vivo* validated enhancers[35], HyDrop v2 model uncovers most tested
524 enhancers while we see a slightly higher performance of the 10x model which was, however,
525 optimized in model architecture and finetuned.

526 Previous benchmarking studies have shown that method comparison is not trivial when
527 many factors (e.g., library preparation, barcoding platform, sequencing depth, processing,
528 annotation resolution) have to be taken into account[19]. Here, the variability of models with and
529 without finetuning adds an additional variable. Besides, the difference observed in the
530 performance of HyDrop v2 and 10x S2F models may be due to differences between the data sets,
531 for example, the 10x dataset had been curated to include only motor cortex cell types, while the
532 HyDrop dataset does not differentiate between endothelial cells or vascular leptomeningeal cells
533 (VLMC), vasoactive intestinal polypeptide reactive interneurons (VIP) or their *SNCG*-positive
534 subtype, and Sst (somatostatin-expressing) cells and their *Calb2*-positive subtype (SstChodl).
535 These cell types were investigated separately by the test enhancer set; thus, the difference in
536 annotation resolution might underlie the slightly lower of the HyDrop v2 model. That makes it even
537 more remarkable that the HyDrop v2 S2F model with a default CREsted architecture scores
538 almost comparable to the 10x model that performed among the best across other earlier tested
539 models in a worldwide community challenge[12] emphasizing the usability of HyDrop v2 to train
540 deep learning models.

541 To, nevertheless, address the sources of variability, we generated parallel datasets in
542 terms of library preparation protocol, data processing, and annotation of the *Drosophila* embryo.
543 We then trained analogous models with 10-fold cross-validation to also factor in the model
544 variability of S2F models. Additionally, most deep learning studies[12,13,21] focus on cell lines or
545 tissues of larger model organisms such as mice, resulting in a lack of evaluation of tools applied
546 to data from non-vertebrate model organisms. Here, we trained S2F model on HyDrop v2 and
547 10x v2 data of the *Drosophila* embryo with (1) data generated with the same library preparation
548 protocol, (2) the same model architecture and (3) comparable cell numbers. With the 10x v2 and
549 HyDrop v2 models, we were equally able to pinpoint the enhancers within *in vivo* tested regions

550 of ~2kb size, in late-stage embryos. The 10-fold cross-validation shows that there is indeed
551 variability between S2F models in cell type-specific accessibility prediction but we, nevertheless,
552 observe a large agreement between the cross-validations in enhancer region selection. With motif
553 enrichment analysis and deep learning-based *de novo* motif discovery, we replicate earlier
554 findings, underscoring the ability of HyDrop v2 data to uncover biological relevant information
555 comparable to 10x just as in mouse.

556 Additionally, we compared both our *Drosophila* S2F models (HyDrop v2 and 10x v2) to a
557 previously published model that was trained on sciATAC-seq3 data, a plate-based assay[15,27]. The
558 five models by de Almeida et al. (2023), one per target tissue, had been finetuned with additional
559 *in vivo* enhancer assays, as opposed to our models that are trained on scATAC-seq data only. In
560 mouse, it has been shown that the recent advances in S2F model design allow for improved
561 models without the need for additional finetuning based on additional data modalities[12]. Models
562 trained on additional data modalities in mouse are evaluated elsewhere[12]. Besides differences in
563 model design, de Almeida et al. (2023) are trained on data of 10-12h of embryo development[15],
564 while our models are trained on a slightly later developmental stage of *Drosophila* development.
565 Additionally, the sciATAC-based models focus on CNS, brain only, epithelial cells, gut cells, and
566 muscle cells while our models include the entire embryo. As especially CNS development
567 undergoes major changes (i.e., the embryonic wave of neurogenesis) in the last hours of embryo
568 development[30], we do not include the CNS and brain models by de Almeida et al. (2023) in our
569 comparison. The synthetic enhancer sequences designed for gut, epidermis, and muscle tissue[15]
570 are identified as target sequences matching the respective cell types in our multi-class model. For
571 muscle, the annotation in our data allows for specifying the synthetic enhancer for the muscle to
572 be active in the somatic muscle tissue, which is also confirmed by the enhancer's *in vivo* validation
573 score[15]. Here, also *de novo* motif discovery driven by our S2F HyDrop v2 model uncovers different
574 motifs important in somatic versus visceral muscles.

575 It becomes apparent that the larger fragments of the sciATAC data cover a wider range of
576 regions compared to 10x v2 and HyDrop v2 when using the same pre-processing. Regarding
577 DARs and motif enrichment, sciATAC only slightly underperforms or achieves equal results as
578 10x and HyDrop v2. The larger fragment size of sciATAC, however, might underlie the need for
579 finetuning of the sciATAC-based S2F model by de Almeida et al. (2023) and the difficulty of
580 integrating sciATAC data with HyDrop v2 and 10x v2 data of the same developmental time stage
581 in our hands. In contrast to sciATAC, HyDrop v2 and 10x v2-based data in *Drosophila* resemble
582 the mouse genome coverage used for successful model generation in mouse[12,13], cell lines[36], or

583 the adult fly[36,37]. This finding underscores the need for a priori evaluation of the input data for deep
584 learning models.

585 Besides investigating the performance of HyDrop v2 data in bioinformatics tools such as
586 motif enrichment and more advanced S2F models, we compared footprints found in 10x and
587 HyDrop v2 data for mouse and fly. In both model organisms, seq2PRINT[34] identifies similar multi-
588 scale footprints, highlighting the wide range of applications that can be reliably performed with
589 data generated with the improved HyDrop v2 assay.

590 Additional comparisons of other scATAC platforms, such as microwell encapsulation of
591 single cells (BD Rhapsody) or well-based combinatorial indexing strategy (Scale Bioscience) for
592 deep learning purposes might be needed to benchmark S2F modeling across a diverse range of
593 experimental techniques. Another plate-based platform called SPATAC is used for zebrafish[38]
594 data generation. In the recent CREsted implementation, the authors show that SPATAC data
595 yields enough information to train S2F models and synthetic enhancer design[22]. To our
596 knowledge, no data for *Drosophila* or mouse cortex generated with SPATAC is available to
597 compare to droplet- and other plate-based platforms.

598 With HyDrop v2, we offer an accessible, scalable, and low-cost method to generate large-
599 scale scATAC-seq datasets suitable for training read-to-use deep learning tools (S2F models and
600 footprinting) without the immediate need for further finetuning. We demonstrate that HyDrop v2
601 data reliably captures biologically relevant regulatory features and can achieve predictive
602 performance comparable to commercial tools such as 10x Genomics. In combination with the
603 easy-to-interpret bioinformatic tools, HyDrop v2 makes gaining biological insights by generating
604 high-quality and low-cost data scATAC more accessible to a wider range of researchers. The
605 integrability of HyDrop v2 data with 10x Genomics data allows for cost-effective upscaling of data
606 generation across species.

607 By providing an evaluation of droplet-based scATAC-seq strategies to generate high-
608 quality training data, we contribute to the improvement of S2F models and other bioinformatics
609 applications. We further exemplify the importance of close interactions between data generation
610 technologies and machine learning in biology. The advances in S2F models to learn the enhancer
611 grammar underlying cell type-specific CREs enable researchers to design synthetic
612 enhancers[15,22,36] targeting specific cell types only. Improving the data generation of large-scale
613 atlases will elevate the design of reliable synthetic enhancers that could be used to develop novel
614 disease treatment strategies. With the increased availability of deep learning tools, future
615 benchmarking studies may be needed to reevaluate newly available bioinformatics tools on their
616 performance on large-scale datasets, ideally composed of data generated on different platforms

for cost-effective use of resources. Our results underscore the importance of evaluating scATAC data across platforms, paving the way for future benchmarking studies to ensure broad generalizability and reproducibility of deep learning approaches in regulatory genomics.

Data availability

The scATAC coverage bigwigs can be downloaded at https://ucsctracks.aertslab.org/papers/hydrop_v2_paper/. The sequencing data and count matrix are available at Gene Expression Omnibus accession number GSE293575. For mouse cortex data, this includes the public data for mouse cortex downloaded from 10x Genomics (https://www.10xgenomics.com/datasets/fresh-cortex-from-adult-mouse-brain-p-50-1-standard-1-1-0, https://www.10xgenomics.com/datasets/8k-adult-mouse-cortex-cells-atac-v1-1-chromium-x-1-1-standard, https://www.10xgenomics.com/datasets/8k-adult-mouse-cortex-cells-atac-v2-chromium-controller-2-standard) and earlier published data of De Rop et al. (2022) with raw data available at GSE175684. The sciATAC-seq data of the Drosophila embryo age 16-20h after egg laying were downloaded from Calderon et al. (2022). All processed fragment files are available at https://resources.aertslab.org/papers/hydrop_v2/.

Code availability

A detailed explanation of the PUMATAC pipeline to process HyDrop v2 and 10x data can be found at https://github.com/aertslab/PUMATAC. All data analysis and model training scripts will become available at https://github.com/aertslab/. Detailed instructions on CREsted can be found at https://github.com/aertslab/CREsted and https://crested.readthedocs.io/en/latest/changelog.html . For Seq2PRINT (scPRINTER in python implementation), we refer to the tutorial found here https://github.com/buenrostrolab/scPrinter by Hu et al. (2025).

References

1. Buenrostro, J. D. *et al.* Single-cell chromatin accessibility reveals principles of regulatory variation. *Nature* **523**, 486–490 (2015).
2. Bartosovic, M. & Castelo-Branco, G. *Multimodal Chromatin Profiling Using Nanobody-Based Single-Cell CUT&Tag*. http://biorxiv.org/lookup/doi/10.1101/2022.03.08.483459 (2022) doi:10.1101/2022.03.08.483459.
3. Robertson, G. *et al.* Genome-wide profiles of STAT1 DNA association using chromatin immunoprecipitation and massively parallel sequencing. *Nat. Methods* **4**, 651–657 (2007).
4. Skene, P. J. & Henikoff, S. An efficient targeted nuclease strategy for high-resolution mapping of DNA binding sites. *eLife* **6**, e21856 (2017).
5. Bravo González-Blas, C. *et al.* cisTopic: cis-regulatory topic modeling on single-cell ATAC-seq data. *Nat. Methods* **16**, 397–400 (2019).
6. Hu, Y. *et al.* Single-cell multi-scale footprinting reveals the modular organization of DNA regulatory elements. 2023.03.28.533945 Preprint at https://doi.org/10.1101/2023.03.28.533945 (2023).
7. Ashuach, T., Reidenbach, D. A., Gayoso, A. & Yosef, N. PeakVI: A deep generative model for single-cell chromatin accessibility analysis. *Cell Rep. Methods* **2**, 100182 (2022).
8. Lalanne, J.-B. *et al.* Multiplex profiling of developmental enhancers with quantitative, single-cell expression reporters. 2022.12.10.519236 Preprint at https://doi.org/10.1101/2022.12.10.519236 (2022).
9. Zhang, K., Zemke, N. R., Armand, E. J. & Ren, B. A fast, scalable and versatile tool for analysis of single-cell omics data. *Nat. Methods* 1–11 (2024) doi:10.1038/s41592-023-02139-9.
10. González-Blas, C. B. *et al. SCENIC+: Single-Cell Multiomic Inference of Enhancers and Gene Regulatory Networks*. http://biorxiv.org/lookup/doi/10.1101/2022.08.19.504505 (2022) doi:10.1101/2022.08.19.504505.
11. Badia-i-Mompel, P. *et al.* Comparison and evaluation of methods to infer gene regulatory networks from multimodal single-cell data. 2024.12.20.629764 Preprint at https://doi.org/10.1101/2024.12.20.629764 (2024).
12. Johansen, N. J. *et al.* Evaluating Methods for the Prediction of Cell Type-Specific Enhancers in the Mammalian Cortex. 2024.08.21.609075 Preprint at https://doi.org/10.1101/2024.08.21.609075 (2024).
13. Hecker, N. *et al.* Enhancer-driven cell type comparison reveals similarities between the mammalian and bird pallium. 2024.04.17.589795 Preprint at https://doi.org/10.1101/2024.04.17.589795 (2024).
14. Taskiran, I. I., Spanier, K. I., Christiaens, V., Mauduit, D. & Aerts, S. *Cell Type Directed Design of Synthetic Enhancers*. http://biorxiv.org/lookup/doi/10.1101/2022.07.26.501466 (2022) doi:10.1101/2022.07.26.501466.
15. de Almeida, B. P. *et al.* Targeted design of synthetic enhancers for selected tissues in the Drosophila embryo. *Nature* 1–5 (2023) doi:10.1038/s41586-023-06905-9.
16. De Winter, S., Konstantakos, V. & Aerts, S. Modelling and design of transcriptional enhancers. *Nat. Rev. Bioeng.* 1–16 (2025) doi:10.1038/s44222-025-00280-y.
17. Kvon, E. Z. *et al.* Genome-scale functional characterization of Drosophila developmental enhancers in vivo. *Nature* **512**, 91–95 (2014).
18. de Almeida, B. P., Reiter, F., Pagani, M. & Stark, A. DeepSTARR predicts enhancer activity from DNA sequence and enables the de novo design of synthetic enhancers. *Nat. Genet.* **54**, 613–624 (2022).
19. De Rop, F. V. *et al.* Systematic benchmarking of single-cell ATAC-sequencing protocols. *Nat. Biotechnol.* 1–11 (2023) doi:10.1038/s41587-023-01881-x.

20. De Rop, F. V. *et al.* Hydrop enables droplet-based single-cell ATAC-seq and single-cell RNA-seq using dissolvable hydrogel beads. *eLife* **11**, e73971 (2022).
21. Pampari, A. *et al.* ChromBPNet: bias factorized, base-resolution deep learning models of chromatin accessibility reveal cis-regulatory sequence syntax, transcription factor footprints and regulatory variants. 2024.12.25.630221 Preprint at https://doi.org/10.1101/2024.12.25.630221 (2025).
22. Kempynck, N. *et al.* CREsted: Cis Regulatory Element Sequence Training, Explanation, and Design. Zenodo https://doi.org/10.5281/zenodo.15045960 (2025).
23. Denisin, A. K. & Pruitt, B. L. Tuning the Range of Polyacrylamide Gel Stiffness for Mechanobiology Applications. *ACS Appl. Mater. Interfaces* **8**, 21893–21902 (2016).
24. Li, Y. E. *et al.* An atlas of gene regulatory elements in adult mouse cerebrum. *Nature* **598**, 129–136 (2021).
25. Ben-Simon, Y. *et al.* A suite of enhancer AAVs and transgenic mouse lines for genetic access to cortical cell types. *bioRxiv* 2024.06.10.597244 (2024) doi:10.1101/2024.06.10.597244.
26. Schreiber, J. jmschrei/tfmodisco-lite. (2025).
27. Calderon, D. *et al.* The continuum of Drosophila embryonic development at single-cell resolution. *Science* **377**, eabn5800 (2022).
28. Domcke, S. *et al.* A human cell atlas of fetal chromatin accessibility. *Science* **370**, eaba7612 (2020).
29. Homem, C. C. F. & Knoblich, J. A. Drosophila neuroblasts: a model for stem cell biology. *Development* **139**, 4297–4310 (2012).
30. Nguyen, P.-K. & Cheng, L. Y. Non-autonomous regulation of neurogenesis by extrinsic cues: a *Drosophila* perspective. *Oxf. Open Neurosci.* **1**, kvac004 (2022).
31. Xiao, Q., Komori, H. & Lee, C.-Y. klumpfuss distinguishes stem cells from progenitor cells during asymmetric neuroblast division. *Development* **139**, 2670–2680 (2012).
32. Jacobs, J. *et al.* The transcription factor Grainyhead primes epithelial enhancers for spatiotemporal activation by displacing nucleosomes. *Nat. Genet.* **50**, 1011–1020 (2018).
33. Nakagoshi, H. Functional specification in the Drosophila endoderm. *Dev. Growth Differ.* **47**, 383–392 (2005).
34. Hu, Y. *et al.* Multiscale footprints reveal the organization of cis-regulatory elements. *Nature* 1–8 (2025) doi:10.1038/s41586-024-08443-4.
35. Adams, M. D. *et al.* The Genome Sequence of Drosophila melanogaster. *Science* **287**, 2185–2195 (2000).
36. Taskiran, I. I. *et al.* Cell-type-directed design of synthetic enhancers. *Nature* 1–9 (2023) doi:10.1038/s41586-023-06936-2.
37. Janssens, J. *et al.* Decoding gene regulation in the fly brain. *Nature* **601**, 630–636 (2022).
38. Sun, K. *et al.* Mapping the chromatin accessibility landscape of zebrafish embryogenesis at single-cell resolution by SPATAC-seq. *Nat. Cell Biol.* 1–13 (2024) doi:10.1038/s41556-024-01449-0.
39. Wang, Y. *et al.* Dissolvable Polyacrylamide Beads for High-Throughput Droplet DNA Barcoding. *Adv. Sci.* **7**, 1903463 (2020).
40. Juzenas, S. *et al.* inDrops-2: a flexible, versatile and cost-efficient droplet microfluidic approach for high-throughput scRNA-seq of fresh and preserved clinical samples. *Nucleic Acids Res.* **53**, gkae1312 (2025).
41. Di Tommaso, P. *et al.* Nextflow enables reproducible computational workflows. *Nat. Biotechnol.* **35**, 316–319 (2017).
42. Korsunsky, I. *et al.* Fast, sensitive and accurate integration of single-cell data with Harmony. *Nat. Methods* **16**, 1289–1296 (2019).

43. Li, H. *et al.* Fly Cell Atlas: A single-nucleus transcriptomic atlas of the adult fruit fly. *Science* **375**, eabk2432 (2022).
44. Thorvaldsdóttir, H., Robinson, J. T. & Mesirov, J. P. Integrative Genomics Viewer (IGV): high-performance genomics data visualization and exploration. *Brief. Bioinform.* **14**, 178–192 (2013).
45. Ramírez, F. *et al.* deepTools2: a next generation web server for deep-sequencing data analysis. *Nucleic Acids Res.* **44**, W160–W165 (2016).
46. Zemke, N. R. *et al.* Conserved and divergent gene regulatory programs of the mammalian neocortex. *Nature* **624**, 390–402 (2023).

Funding

ERC-AdG (101054387), CZI (DI2-0000000068), and SBO (S005024N) to S.A, VIB Tech Watch funding to S.P, FWO fellowship to H.D. (1168625N), FWO fellowship to F.D.R. (1S80920N), FWO PhD fellowship to N.K. (1SH6J24N). This research was funded in part by Aligning Science Across Parkinson's [ASAP-000430 and ASAP-025179] through the Michael J. Fox Foundation for Parkinson's Research (MJFF).

License

For the purpose of open access, the author has applied a CC BY public copyright license to all Author Accepted Manuscripts arising from this submission.

Declaration of competing interest

The authors declare the absence of competing interests.

Author's contributions

Conceptualization: S.P., H.D., S.A.
HyDrop bead design & generation: S.P., M.W.
Computational analysis: H.D., L.K., E.C.E., N.K.
Data collection, processing, and curation: H.D., F.D.R., G.H.
Experiments and sample preparation: K.T., F.D.R, V.C., H.D., N.R., K.S., R.V.
Resources: S.A., S.P.
Visualization: H.D., S.P., K.T.
Writing: H.D., S.P., K.T.

Acknowledgments

We thank the members of the Laboratory of Computational Biology for their feedback during the process of method improvement and data collection. We thank Jean-Christophe Marine for his kind donation of the mouse melanoma lines. Lastly, we thank the staff of the Flemish Supercomputing Center (Vlaams Supercomputer Centrum - VSC) and VIB Data Core for their support.

KEY RESOURCES TABLE

See supplementary material Table S1.

STAR Methods

EXPERIMENTAL MODEL AND STUDY PARTICIPANT DETAILS

Drosophila lines

The DGRP fly lines (DGRP-639, DGRP-502, DGRP-409) were purchased from Bloomington (25199, 28204, and 28278 respectively).

Mouse lines

Cortical brain tissue from female P60 with C57B/6J background was used. The experiments were conducted in line with KU Leuven's ethical guidelines and approved by the Ethical Committee for Animal Experimentation (protocol number P007/2021).

Cell lines

For the barnyard test of HyDrop v2, cells from a human breast cancer cell line (MCF-7; RRID:CVCL_0031) and mouse melanoma cells were mixed. The use of the cell lines was approved by the KU Leuven Ethical Committee under project number S63316.

METHOD DETAILS

Barcoded hydrogel bead manufacturing and storage

The microfluidic droplet generators for HyDrop v2 were produced following the previously described protocol[20] modified as described below. A detailed protocol can be found at http://dx.doi.org/10.17504/protocols.io.8epv5n11dv1b/v1.

783 Dissolvable hydrogel beads for HyDrop v2 are synthesized similarly to previously
784 published protocols[20,39] and barcoded by three rounds of split-and-pool ligation reactions[40]. For
785 synthesizing 2–3 mL batch of beads, 1.1 mL of Bead Monomer Mix (8.5-10% acrylamide (%T),
786 2-4% bisacryloylcystoylamine (%C), 10% Tris-buffered saline with EDTA and Triton X-100
787 (TBSET) (10 mM Tris-HCl pH 8, 137 mM NaCl, 2.7 mM KCl, 10 mM EDTA, 0.1% Triton X-100),
788 4 μM acrydite primer, 0.6% ammonium persulfate) was encapsulated into 60 μm diameter
789 droplets in HFE-7500 Novac oil with EA-008 surfactant (RAN Biotech) with 0.5% TEMED. Flow
790 rates: monomer: 400 and oil 750. The resulting emulsion was collected into 2 low bind 1.5 mL
791 Eppendorf, layered with 200 μL mineral oil, and incubated at 65 °C for 14 hours, then paused at
792 12 °C. Excess mineral oil and the emulsion oil were removed and three washes with 1 mL of
793 droplet-breaking solution (20% PFO in HFE) were performed. Beads were pelleted at 1000 xg, 4
794 °C for 60 seconds and washed three times in 1 mL of 1% SPAN-80 in hexane (0.2μm syringe
795 filter). Beads were sequentially washed three times with TBSET and three times with TET buffer.
796 Bead QC was performed as described previously (Zilionis et al., 2017; De Rop et al., 2022) and
797 beads were filtered using a 70 μm filter (EASYstrainer from Greiner) to exclude large bead
798 contamination. The beads are stored in TET buffer at 4 °C.
799 For barcoding round one, on the day of barcoding, the beads were first washed with TET
800 buffer by spinning down (3 minutes at 1000 xg, gentle braking), discarding supernatant, and
801 resuspension in TET buffer. After centrifugation, the TET buffer was removed, and the beads
802 were washed two times with pre-ligation buffer (10 mM Tris-HCl pH. 8.0, 30 mM NaCl, 1 mM
803 $MgCl_2$ 0.1% Tween-20) for 1 minute at 1000 xg with gentle braking. After washing the supernatant
804 was removed to obtain a compacted pellet of beads. A Hamilton microlab STAR robot was used
805 for liquid handling in the deep well 96-well plates during barcoding. 22 μL of compacted beads
806 was aliquoted in each well of the 96-well plate. Next, 16 μL of 2× ligation-primer buffer (100 mM
807 Tris-HCl pH 7.5, 20 mM $MgCl_2$) and 4 μL oligo mix cassette (200 μM) were added. The plate was
808 spun, the contents mixed by vortexing, spun again, and placed on a PCR block (pre-heated to 75
809 °C with heated lid at 105 °C). To anneal the oligos the heating was turned off after 3 minutes at
810 75 °C which allowed gradual cooling to room temperature (about 2.5 hours). During this cooling
811 process, the plate is taken off the PCR-block and vortexed every 30 minutes at 2000 RPM to
812 resuspend the beads. When the temperature reached 33 °C the plate was left at room
813 temperature for 10 minutes. The Mantis (Formulatrix) was used to aliquot 10 μL ligase mix (50
814 mM Tris-HCl pH 7.5, 10 mM $MgCl_2$, 5.1 mM ATP, 100 U/μL T4 ligase (New England Biolabs)) to
815 each well. Plates were sealed, vortexed in a vortex shaker and centrifuged for 30 seconds at 1000
816 xg. Then the beads were mixed on a thermoblock shaker for 30 seconds at 2000 RPM. Ligation

817 was performed for 60 minutes at 25 °C with shaking alternating between 1000 and 1600 RPM for
818 30 seconds each. Afterwards, the plate was incubated overnight at 16 °C on a thermoblock while
819 being shaked at 1000 RPM. After the overnight incubation, the plate was kept at 4 °C for at least
820 30 minutes before we proceeded with the inactivation of the ligation by performing a cleanup step
821 on the Hamilton with STOP-25 (10 mM Tris-HCl pH 8, 25 mM EDTA, 0,10% Tween-20, 100 mM
822 KCl). The beads were transferred to a 50 mL falcon and incubated for 20 minutes. Afterward, the
823 beads were spun down (3220 xg for 7 minutes, gentle braking), the supernatant was removed,
824 and the beads were transferred to a 15 mL tube. Next the beads were washed once with STOP-
825 10 (10 mM Tris-HCl pH 8, 10 mM EDTA, 0.10% Tween-20, 100 mM KCl) and three times with
826 TET buffer (centrifugation at 1000 xg for 1 minute). The second round of barcoding was started
827 after two washes with pre-ligation buffer (centrifugation at 1000 xg for 1 minute) after which we
828 transferred 22 µL compacted beads to each well of a 96-well plate.

829 For the round 2 barcoding, the 4 µL of the barcode 2 oligo cassette is added to 16 µL of
830 2× ligation-primer buffer in a 96-well plate and annealing is achieved again with a PCR-block.
831 Afterwards, the plate is spun to collect the condensate. The annealed cassettes were then
832 transferred to the bead plate. Ligation was performed as discussed in barcode step one.

833 Barcoding step 3 was done like step 1 with the exception that 23 µL of compacted beads
834 was aliquoted in each well and mixed with 17 µL of 2× ligation-primer buffer and 3 µL of barcode
835 3 oligo mix (500 µM).

836 The barcoded beads are cleaned one last time on the Hamilton with STOP-25 buffer as
837 described above and denatured with denaturation buffer (0.1 N NaOH, 1.68% Brij-35) for 10 min
838 at room temperature at rotation (1 minute at 1000 xg). The beads are then washed with the
839 neutralization buffer (100 mM Tris HCl pH 8, 10 mM EDTA, 0.1% Tween-20, 100 mM NaCl) for
840 10 min at room temperature with rotation (1 minute at 1000 xg). Finally, the beads are washed 3
841 times with TET buffer (1 minute at 1000 xg) and filtered twice using 70 um cell strainers.

842 The barcoded and cleaned beads are then incubated overnight at 4 °C in lysis buffer (125
843 mM Tris HCl pH 7, 150 mM NaCl, 12.5 mM $MgCl_2$, 1.25% Triton X-100, 0.4% BSA). The beads
844 are washed twice more with lysis buffer (1 minute at 1000 xg) and aliquoted into capped PCR-
845 strip tubes (40 µL) and stored at –80 °C.

846 Sanger sequencing of barcoded beads

847 To test the purity of our barcoded HyDrop v2 beads, 1 µL of finalized barcoded beads was
848 taken from their storage at -80 °C and they were pelleted and washed three times with 0.04%
849 BSA in PBS in a 1.5 mL microcentrifuge tube (centrifuge for 1 minute at 500 xg). The beads were
850 diluted with PBS/BSA under a stereo microscope (Leica S8 APO) on a petri dish (Falcon 351008)

851 until individual beads could be picked with a Stripper® pipette and 75 µm capillaries (MXL3-STR
852 and MXL3-75, CooperSurgical). Individual beads were transferred consequently over three drops
853 (5 to 10 µL) to ensure no other beads were present in the capillary. Next, single beads, in 0.5 µL
854 of PBS/BSA, were transferred to PCR tubes containing 1.5 µL PBS/BSA. Afterwards, the capillary
855 was washed three times in a large volume of PBS/BSA.

856 To the picked beads in the PCR tube, 18 µL PCR master mix was added (final
857 concentrations: 1× KAPA HiFi hot start ready mix (Roche Cat. No. KK2602), 30 mM DTT, 1 µM
858 ATAC-QC oligo) and the following PCR program was used: 72 °C – 3 mins, 98 °C – 30 s, 22
859 cycles of 98 °C – 10 s; 59 °C – 30 s; 72 °C – 30 s; and finally the amplification products were
860 cooled to 4 °C. This product was purified using 1.5× Ampure XP beads and the washed beads
861 were resuspended in 10 µL of EB buffer (Qiagen) and 8 µL of the eluate was used in the next
862 PCR reaction (total volume is 20 µL with final concentrations: 1× KAPA HiFi hot start ready mix,
863 1 µM P7 primer, 1 µM P5 primer). Sanger sequencing was done by LGC Genomics using the P7
864 primer.

865 To test HyDrop v1 bead purity the same protocol was followed but different oligos were
866 used (see Table S1).

867 Husbandry and sample extraction

868 Mouse

869 The mice with C57B/6J background were housed under standard housing conditions in a
870 pathogen-free facility with a 14 hr light, 10 hr dark light cycle from 7 to 21 hr. Mice used in the
871 study were 60 days old. Animals were euthanized using 0.05 mL/g BodyWeight. The chest cavity
872 was opened, and the brains were flushed with 5 mL PBS through the left ventricle of the heart
873 followed by decapitation. Brains were dissected out and cortices were collected. The motor cortex
874 is dissected, snap-frozen in liquid nitrogen, and stored at -80 °C.

875 Nuclei extraction

876 Mouse nuclei for HyDrop-ATACv2 and 10x Genomics Single Cell ATAC v2 were extracted
877 from mouse cortex samples that were snap-frozen in liquid nitrogen and stored at -80 °C. We
878 transferred ~1 cm^3 of frozen mouse cortex to 500 µL of ice-cold homogenization buffer (10 mM
879 Tris-HCl pH 7.5, 10 mM NaCl, 3 mM $MgCl_2$, 320 mM sucrose, 0.1 mM EDTA, 0.5% BSA, 0.1%
880 IGEPAL CA-630, 1× complete protease inhibitor, and 1 mM DTT) in a Dounce Homogenizer
881 (KIMBLE, 1 mL). The tissue was left to thaw for 2 min before the tissue was homogenized with
882 10 strokes of the loose pestle and 5 strokes of the tight pestle. Before the end of a 5-minute
883 incubation, the homogenate was filtered through a 70 µm cell strainer (Corning), and the
884 homogenizer and strainer were washed with homogenization buffer to obtain a final volume of 1

885 mL. The filtrate was transferred to a 1.5 mL DNA LoBind tube (Eppendorf) and centrifuged at 500
886 xg for 5 minutes. The supernatant was discarded, and the pellet was topped up to 520 µL with
887 wash buffer 1 (10 mM Tris-HCl pH 7.5, 10 mM NaCl, 3 mM $MgCl_2$, 320 mM sucrose, 0.1 mM
888 EDTA, 0.5% BSA, 1× complete protease inhibitor, and 1 mM DTT) and resuspended. Next, we
889 added 520 µL gradient medium (50% Optiprep, 10 mM Tris-HCl pH 7.5, 1 mM $CaCl_2$, 5 mM $MgCl_2$,
890 75 mM sucrose, 1× complete protease inhibitor, and 1 mM DTT) and mixed the entire volume by
891 gentle pipetting. In a 2 mL DNA LoBind tube (Eppendorf) we layered 790 µL Optiprep cushion
892 (29% Optiprep, 31 mM Tris-HCl pH 8, 77.5 mM KCl, 15.5 mM $MgCl_2$, 129.2 mM sucrose) at the
893 bottom and 1040 µL of the sample on top, gently without disrupting the cushion. The tube was
894 then centrifuged at 9000 xg for 20 minutes at 4 °C. After the centrifugation the debris on top was
895 carefully removed with a 1 mL tip and the rest of the supernatant was also carefully removed until
896 50 µL was left in the tube. The pellet was gently resuspended before we mixed it with 50 µL 2×
897 permeabilization buffer (20 mM Tris-HCl pH 7.5, 20 mM NaCl, 6 mM $MgCl_2$, 0.2% Tween-20,
898 0.02% IGEPAL CA-630, 0.02% Digitonin, 2% BSA, and 2 mM DTT) and left the nuclei suspension
899 for 2 minutes on ice before we stopped the permeabilization by mixing it with 1 mL of wash buffer
900 2 (10 mM Tris-HCl pH 7.5, 10 mM NaCl, 3 mM $MgCl_2$, 0.1% Tween-20, 1% BSA). The nuclei were
901 pelleted by centrifugation at 500 xg for 5 minutes at 4 °C. The nuclei were resuspended in PBS
902 with 0.04% BSA for HyDrop-ATAC v2 and in Diluted Nuclei Buffer for 10x Genomics Single Cell
903 ATAC v2 processing.

904 Fly

905 All flies were raised on a yeast-based medium and kept at 25 °C on a 12h/12h day/night
906 light cycle. For embryo collection, flies were transferred to cages fixed to a plate with a normal
907 yeast-based medium 24 hours before embryo collection. On the day of embryo collection, the
908 plate was exchanged for a juice plate. The juice was prepped by adding 20 g agar and 22 g
909 sucrose to 300 ml distilled water, boiling, and then mixing in 100 ml apple juice, 10 ml 95%
910 ethanol, and 5 ml 100% glacial acetic acid. The flies laid eggs for four hours. Sixteen hours later,
911 the embryos aged between 16 to 20 hours were collected from the juice plate with a small brush
912 and transferred to a 70 µm nylon mesh filter. To dechorionate the embryos, the embryos were
913 treated for 2 min with 5% bleach and then washed 4 times with 0.1% Triton X-100 in 1× PBS.
914 After a final wash in 1× PBS, the embryos were transferred to a 1.5 ml tube, spun down for 2 min
915 at 500 g, supernatant was removed, and the embryo pellet was snap frozen on dry ice and stored
916 at -80°C.

917 Nuclei extraction

918 Nuclei were isolated by using an adapted protocol based on the nuclei isolation protocol
919 for single-cell ATAC sequencing (10x Chromium CG000169-RevE). Briefly, the embryos were
920 resuspended in 500 µl cold lysis buffer (10 mM Tris-HCl pH 7.4, 10 mM NaCl, 3 mM $MgCl_2$, 0.1%
921 Tween-20, 0.1% IGEPAL CA-630, 0.01% Digitonin, 1% BSA), transferred to a Dounce
922 homogenizer and incubated on ice for 5 minutes. The tissue was disrupted by 25 strokes with the
923 loose pestle, incubated on ice for 10 minutes, and disrupted by 25 strokes with the tight pestle.
924 To remove debris, the solution was filtered on a 10 µm nylon mesh filter and washed with 1 ml
925 wash buffer (10 mM Tris-HCl pH 7.4, 10 mM NaCl, 3 mM $MgCl_2$, 0.1% Tween-20, 1% BSA).
926 Nuclei were collected by centrifugation at 500 g for 5 mins at 4°C, supernatants were carefully
927 removed, and nuclei were resuspended in 50 µl 1× Diluted Nuclei Buffer (10x Chromium). Nuclei
928 quality and concentration were assessed by the LUNA-FL Dual Fluorescence Cell Counter.

929 Cell lines

930 For a detailed description of cell culture and cell dissociation see De Rop (2022). In brief,
931 MCF-7 cells (NCI-DTP Cat# MCF7, RRID:CVCL_0031) were cultured in RPMI1640
932 (ThermoFisher 11875093) medium supplemented with 10% FBS (ThermoFisher 10270–106), 1%
933 penicillin/streptomycin (Life Technologies 15140122), and 10 ug/mL insulin (Sigma Aldrich I9278)
934 and passaged twice per week. Mouse melanoma cells were cultured in DMEM (ThermoFisher
935 13345364) supplemented with 10% FBS and 1% penicillin/streptomycin and passaged once per
936 week. All cell lines tested negative for mycoplasma prior to use. Cells were washed in PBS and
937 dissociated into single-cell suspensions by adding 1.5 mL of 0.05% trypsin (Life Technologies
938 25300054) and waiting for 5 minutes. The single-cell suspension was centrifuged at 500 rcf for 5
939 min at 4°C and the resulting pellet was resuspended in PBS. This PBS wash was repeated once
940 more and the single-cell suspension was processed further.

941 Nuclei extraction

942 For the barnyard, the cell lines were mixed to equal parts and a pellet of one million
943 dissociated cells or fewer was incubated on ice in 200 µL of ATAC lysis buffer (1% BSA, 10 mM
944 Tris-HCl pH 7.5, 10 mM NaCl, 0.1% Tween-20, 0.1% NP-40, 3 mM $MgCl_2$, 70 µM Pitstop in
945 DMSO, 0.01% digitonin) for 5 minutes. 1 mL of ATAC nuclei wash buffer (1% BSA, 10 mM Tris-
946 HCl pH 7.5, 0.1% Tween-20, 10 mM NaCl, 3 mM $MgCl_2$) was added and the nuclei were pelleted
947 at 500 xg, 4 °C for 5 minutes. The resulting pellet was resuspended in 100 µL of ice-cold PBS
948 and filtered with a 40 µm strainer (Flowmi).

949 ## HyDrop-ATAC v2 library preparation

950 A detailed description of the protocol can be found here
951 dx.doi.org/10.17504/protocols.io.x54v97mmpg3e/v1.

952 ### Mouse

953 Between 7500 and 18000 nuclei, resuspended in PBS (supplemented with 0.04% BSA),
954 were tagmented for one hour at 37 °C in 15 µL ATAC reaction mix (10% DMF, 10 mM Tris-HCl
955 pH 7.4, 5 mM $MgCl_2$, 5 ng/µL Tn5, 70 µM Pitstop in DMSO, 0.1% Tween-20, 0.01% Digitonin).
956 Tagmented nuclei were placed on ice and 95 µL of PCR mix (1.25× Phusion HF buffer, 15%
957 Optiprep, 1.25 mM dNTPs, 75 mM DTT, 0.0625 U/µL Phusion HF polymerase, 0.0625 U/µL Deep
958 Vent polymerase, 0.0125 U/µL ET SSB) was added. Next, 110 µL of nuclei mixed in PCR mix
959 was co-encapsulated with 45 µL of HyDrop-ATACv2 beads in HFE-7500 Novac oil with EA-008
960 surfactant (RAN Biotech) using the Onyx microfluidics platform (Droplet Genomics). The resulting
961 emulsion was split over two PCR tubes and was placed in a thermocycler with the following
962 program: 72 °C – 15 mins, 98 °C – 3 mins, 12 cycles of 98 °C – 10 s; 55 °C – 30 s; 72 °C – 1 min;
963 and a final extension of 72 °C – 5 min, followed by a hold stage at 4 °C.. To break the emulsion
964 and remove excess oil, 125 µL of recovery agent (20% PFO in HFE) was added and the PCR
965 tubes were inverted 10 times to mix before the oily phase was removed. Next, we added 180 µL
966 GITC mix (5M GITC, 25 mM EDTA, 50 mM Tris-HCl pH 7.4), 10 µL Dynabeads, and 10 µL 2.4 M
967 DTT to each of the aliquots, and mixed everything by pipetting up and down 10 times and
968 incubating for 10 minutes. Dynabeads were pelleted on a magnet and washed twice with 80%
969 ethanol. Elution was done in 50 µL of EB-DTT-Tween (24 mM DTT, 0.1% Tween-20 in EB (10
970 mM Tris-HCl pH 8.5)). Next, a 1.2× Ampure bead purification was performed according to
971 manufacturer's recommendations. Elution was done with 40 µL of EB-DTT (10 mM DTT in EB).
972 The library was completed by amplifying the eluate in a total volume of 100 µL PCR mix (1× KAPA
973 HiFi, 1 µM index i7 primer, 1 µM Universal P5 primer) with the following program: 95 °C – 3 mins,
974 12 cycles of 98 °C – 10 s; 63°C – 30 s; 72 °C – 1 min; and a final extension of 72 °C – 1 min,
975 followed by a hold stage at 4 °C. The final libraries were subjected to 0.4×–1.2× doublesided
976 Ampure purification and eluted in 20 µL elution buffer (Qiagen).

977 ### Fly

978 Analogous to mouse nuclei, the HyDrop v2 protocol was performed on the lysed
979 Drosophila nuclei, resuspended in 1x nuclei buffer. A total of 80,000 nuclei were resuspended in
980 40 µL of ATAC reaction mix (10% DMF, 10% Tris-HCl pH 7.5, 5 mM $MgCl_2$, 4.7 ng/µL Tn5, 70
981 µM Pitstop in DMSO, 0.1% Tween-20, 0.01% digitonin) and incubated at 37°C for 1 hr.
982 Tagmented nuclei were placed on ice and counted with the LUNA-FL Dual Fluorescence Cell

983 Counter. Per HyDrop reaction, a total of 37,500 tagmented nuclei were used in a 80 µl PCR
984 reaction (1.37× Phusion HF buffer, 1.37% PEG-8000, 0.68 mM dNTPs, 89 mM DTT, 0.04 U/µL
985 Phusion HF polymerase, 0.04 U/µL Deep Vent polymerase, 0.01 U/µL ET SSB). Next, 80 µL of
986 nuclei mixed in PCR mix was co-encapsulated with 35 µL of HyDrop-ATACv2 beads in HFE-7500
987 Novac oil with EA-008 surfactant (RAN Biotech) using the Onyx microfluidics platform (Droplet
988 Genomics). The resulting emulsion was placed in a thermocycler with the following program: 72
989 °C – 20 mins, 98 °C – 3 mins, 12 cycles of 98 °C – 10 s; 58 °C – 30 s; 72 °C – 1 min; and a final
990 extension of 72 °C – 5 min, followed by a hold stage at 4 °C. To break the emulsion and remove
991 excess oil, 125 µL of recovery agent (20% PFO in HFE) was added and the PCR tube was
992 inverted 10 times to mix before the oily phase was removed. Next, we added 180 µL GITC mix
993 (5M GITC, 25 mM EDTA, 50 mM Tris-HCl pH 7.4), 10 µL Dynabeads Silane One, and 10 µL 2.4
994 M DTT, and mixed everything by pipetting up and down 10 times and incubating for 10 minutes.
995 Dynabeads were pelleted on a magnet and washed twice with 80% ethanol. Elution was done in
996 100 µL of EB-DTT-Tween (24 mM DTT, 0.1% Tween-20 in EB (10 mM Tris-HCl pH 8.5)). Next, a
997 1.1× Ampure bead purification was performed according to manufacturer's recommendations.
998 Elution was done with 40 µL of EB-DTT (10 mM DTT in EB). The library was completed by
999 amplifying the eluate in a total volume of 100 µL PCR mix (1× KAPA HiFi, 1 µM index i7 primer,
1000 1 µM Universal P5 primer) with the following program: 95 °C – 3 mins, 10 cycles of 98 °C – 10 s;
1001 63°C – 30 s; 72 °C – 1 min; and a final extension of 72 °C – 1 min, followed by a hold stage at 4
1002 °C. The final libraries were subjected to 0.4×–1.2× doublesided Ampure purification and eluted in
1003 20 µL elution buffer (Qiagen).
1004 scATAC-seq libraries were prepared according to the Chromium Single Cell ATAC
1005 reagent kits v2 user guide (10x Genomics, CG000496 Rev B). Briefly, the transposition reaction
1006 was prepared by mixing the desired number of nuclei with ATAC Buffer and ATAC Enzyme, and
1007 was then incubated for 30 minutes at 37 °C. Tagmented nuclei were partitioned into nanoliter-
1008 scale gel bead-in-emulsions (GEMs). DNA linear amplification was then performed by incubating
1009 the GEMs under the following thermal cycling conditions: 72 °C – 5 min, 98 °C – 30 s, 12 cycles
1010 of 98 °C – 10 s; 59 °C – 30 s; 72 °C – 1 min, and finally a hold stage at 4 °C. GEMs were broken
1011 using Recovery Agent, and the resulting DNA was purified by sequential Dynabeads and
1012 SPRIselect reagent beads cleanups. Libraries were indexed by PCR using a Single Index kit N
1013 set A and incubated under the following thermal cycling conditions: 98 °C – 45 s, seven cycles of
1014 98 °C – 20 s; 67 °C – 30 s; 72 °C – 20 s; and a final extension of 72 °C – 1 min, followed by a hold
1015 stage at 4 °C. Sequencing libraries were subjected to a final bead cleanup with SPRIselect
1016 reagent.

1017 ## Sequencing

1018 HyDrop-ATAC v2 libraries were sequenced on an Illumina NextSeq2000 or NovaSeqX
1019 system using at least 43 cycles for read 1 (ATAC paired-end mate 1), 10 cycles for index 1
1020 (sample index), 41 cycles for index 2 (HyDrop-ATAC v2 barcode), and 44 cycles for read 2 (ATAC
1021 paired-end mate 2).

1022 ## scATAC data processing

1023 All in-house generated 10x and HyDrop samples were processed using the PUMATAC
1024 pipeline[19] (RRID:SCR_026624), built on Nextflow[41] (v21.04.3; RRID:SCR_024135). With
1025 PUMATAC, we aligned the samples to the mm10 and dm6 reference genomes for mouse and fly
1026 respectively to write fragment files and perform quality assessment. For an in-depth description
1027 of the pipeline, see De Rop et al. (2023)[19] and https://github.com/aertslab/PUMATAC.

1028 ### Barnyard

1029 A mixed library of 5000 mouse melanoma and 5000 MCF-7 cells was generated following
1030 the standard HyDrop v2 library protocol as described above for the mouse cortex. The raw data
1031 was processed using the PUMATAC pipeline[19] and aligned to a combined reference genome for
1032 mm10 and GRCh38. Cut-offs for TSS enrichment and number of unique fragments per cell were
1033 set using the Otsu algorithm. Lastly, the fragments belonging to each genome were counted and
1034 compared.

1035 ### Mouse samples

1036 10x v2 and 10x v1 fastq files were downloaded from 10x Genomics database. The
1037 samples were processed using the PUMATAC pipeline[19], together with the in-house generated
1038 data. Cut-offs were set per sample using the Otsu threshold for TSS enrichment and number of
1039 unique fragments per cell. Next, fragments overlapping earlier published mouse candidate cis-
1040 regulatory regions[24] were combined into a count matrix using pycisTopic[5] (v2.0a0, RRID:
1041 SCR_026618). Potential doublets were removed using Scrublet (RRID:SCR_018098) with an
1042 automatic threshold set based on the expectation of 10% doublets. Cells were clustered based
1043 on initial pycisTopic[5] Latent Dirichlet Allocation (LDA) using 80 topics. Based on this initial
1044 clustering, a new set of consensus regions was generated using MACS2, overlapping fragments
1045 recounted, and assembled into a second count matrix. Again, doublets were removed as
1046 previously and LDA performed with now 130 topics to capture all possible cell types. Artifacts
1047 attributed to batch effects were corrected using Harmony[42] giving the sequencing technique as
1048 variable instead of the sample identifier. Next, based on Leiden resolution 2.5, the cells were
1049 annotated using differentially accessible regions (DARs) of previously published datasets[25,43]. The

1050 newly annotated cell types were subdivided based on the sequencing technique of each sample.
1051 On the new variable, DARs were calculated based on imputed chromatin accessibility. Here, only
1052 regions passing one-versus-all Wilcoxon rank-sum tests with 0.05 adjusted p-value are included.
1053 The top 1000 DARs per cell type per sequencing technique were investigated with motif
1054 enrichment analysis with pyCisTarget[10] (v1.0a2, RRID:SCR_026626). Using pycisTopic[5] to call
1055 peaks per cell type in pseudobulk with MACS2, peak BED files per cell type were generated.

1056 For BigWig files generation per cell type/sequencing technique, the lowest number of cells
1057 in one cell type in the respective sparsest sequencing technique was set as maximum. An equal
1058 number of cells for that cell type was randomly selected per remaining sequencing technique.
1059 Only cell types with more than 100 cells in each sequencing technique were included further on.
1060 Next, BigWig files for fragment coverage and Tn5 cut sites were generated for the downsampled,
1061 equal number of cells per technique with scATAC Fragment Tools (RRID:SCR_026643)
1062 normalizing the genome coverage (divided by the number of fragments. They were visualized
1063 with the integrative genome viewer (IGV, RRID:SCR_011793)[44]. The carrot plots (i.e., heat maps)
1064 were generated with deepTools2[45] (v3.5.3; RRID:SCR_016366) plotting the accessibility per cell
1065 type and sequencing technique (BigWig) on the cell type-specific peak files (i.e., all regions
1066 accessible in that respective cell type). This was done for BigWigs based on fragment coverage
1067 and Tn5 cut sites.

1068 For the comparison of quality metrics across microfluidic techniques, the samples were
1069 downsampled to 36,000 reads per cell (RPC) as indicated in the respective figures. The plots
1070 were generated based on PUMATAC quality control evaluation with cell names defined based on
1071 previous annotations of the full sequencing depth count matrix.

1072 Drosophila samples

1073 Analogous to the mouse cortex data processing, the 10x v2 and HyDrop v2 data were
1074 processed with the PUMATAC pipeline[19]. Cut-offs were set per sample using the Otsu threshold
1075 with a maximum cut-off of 800 unique fragments and a TSS enrichment of 2. Fragments
1076 overlapping candidate regions of the earlier published Drosophila fly embryo dataset[27] were
1077 combined into a count matrix using pycisTopic[5] and clustered with 120 topics. Based on this initial
1078 clustering, a new set of consensus regions was generated with MACS2, overlapping fragments
1079 recounted and assembled into a new count matrix. LDA was performed in pycisTopic[5] with 220
1080 topics and clusters annotated with DARs from the published Drosophila embryo atlas[27] on Leiden
1081 resolution 1.2. Correction of batch effects was performed with Harmony[42] using the respective
1082 wet lab technique (sequencing technique and sample preparation parameter) as variable.
1083 Analogous to the mouse data, the annotated cell types were subdivided among HyDrop v2 and

1084 10x v2. On the new variable, DARs were calculated based on imputed chromatin accessibility.
1085 Here, only regions passing one-versus-all Wilcoxon rank-sum tests with 0.05 adjusted p-value
1086 are included. The top 1000 DARs per cell type per sequencing technique were investigated with
1087 motif enrichment analysis with pyCisTarget[8]. Using pycisTopic[3] to call peaks per cell type in
1088 pseudobulk with MACS2, peak BED files per cell type were generated.

1089 For BigWig files generation per cell type/sequencing technique, the lowest number of cells
1090 in one cell type in the respective sparsest sequencing technique was set as maximum. An equal
1091 number of cells for that cell type was randomly selected per remaining sequencing technique.
1092 Only cell types with more than 1000 cells in each sequencing technique were included further on.
1093 Next, BigWig files for fragment coverage and Tn5 cut sites were generated for the downsampled,
1094 equal number of cells per technique with scATAC Fragment Tools
1095 (https://aertslab.github.io/scatac_fragment_tools/) normalizing the genome coverage (divided by
1096 the number of fragments. They were visualized with the integrative genome viewer (IGV;
1097 RRID:SCR_011793)[44] Just as in mouse, the carrot plots (i.e., heat maps) were generated with
1098 deepTools2[45] for BigWigs based on fragment coverage and Tn5 cut sites.

1099 For the comparison of quality metrics between HyDrop v2 and 10x v2, the samples were
1100 downsampled to 12,000 reads per cell (RPC) as indicated in the respective figures. The plots
1101 were generated based on PUMATAC quality control evaluation with cell names defined based on
1102 previous annotations of the full sequencing depth count matrix.

1103 For the sciATAC data, the available fragment files of two experiments of embryos of 16 to
1104 20 hours after egg laying form the publicly available data from the embryo atlas[27] were
1105 downloaded. Just as previously described, they were scored in two rounds with their own
1106 consensus peaks in the second processing round. Here, the maximum cutoff was just as in 10x
1107 and HyDrop samples set to TSS enrichment of two and 800 unique fragments. The data is
1108 clustered using pycisTopic[5] with 220 topics and previous annotations[27] assigned. Again, DARs
1109 were calculated as previously described, and motif enrichment analysis was performed with
1110 pyCisTarget[8] on the top 1000 DARs. Coverage and cut site BigWig files were calculated
1111 analogous to 10xv2 and HyDrop v2 fly data. No downsampling took place for sciATAC data.

1112 Model training

1113 Mouse

1114 Samples generated with the HyDrop v2 platform were extracted from the count matrix
1115 generated for the integrated samples. Again, using pycisTopic[5], LDA was performed with 100
1116 topics. No batch correction of the HyDrop v2 beads was needed. For downstream training of the
1117 HyDrop v2-based sequence model, pseudobulk profiles were generated in pycisTopic[5] with

1118 MACS2 peak calling based on grouping cells in motor cortex cell types previously annotations of
1119 the full data set.

1120 The sequence model was trained with the CREsted package[22]
1121 (v.1.3.0RRID:SCR_026617) following the default peak regression parameters. Briefly, the data
1122 was divided into validation (chr8, chr10), train (chr 9, chr18), and remaining data and resized to
1123 2,114bp length. Peaks were normalized using the top 2% of the peaks. Next, the data was
1124 augmented with a sequence shift of 3 bp (to both sites) stochastically during training and the use
1125 of the reverse complement previous to model training using the dilatedcnn model architecture.

1126 To compare the HyDrop v2 sequence model to a published and evaluated data set, 10x
1127 multiome data generated with frozen primary motor cortex tissue from eight P56 C57BL/6J male
1128 mice (*Mus musculus*) generated[46] with the 10x protocol was used. The dataset has previously
1129 been annotated and extensively evaluated for deep learning purposes[12,46]. The model was trained
1130 using the standard CREsted peak regression pipeline, by first pretraining on all consensus peaks
1131 and fine-tuning on a set of cell type-specific peaks. Just as in the HyDrop v2 model training, the
1132 same validation and training splits were handled followed by resizing to 2,114bp length. The
1133 peaks were also normalized using the top 3% of the peaks and the data augments as previously
1134 described. Again, the dilatedcnn model architecture was used for the model training.

1135 In both models, recurrent sequence patterns were identified in the top 2,000 regions that
1136 overlapping between 10x and HyDrop v2 data sets per cell type with *tfmodisco-lite* within the
1137 default parameters of the CREsted package.

1138 Patterns between cell types and techniques were compared with the function
1139 *crested.tl.modisco.process_patterns* based on tomtom with the default parameters for similarity
1140 threshold of 3.5, trimming patterns based on an information content of 0.1 and discarding patterns
1141 with a threshold of 0.2.

1142 *In vivo* validated enhancers recovery curves

1143 A set of 122 functionally validated On-Target, mouse genomic enhancer regions in the
1144 mouse motor cortex was taken from a dataset provided by Ben-Simon et al.[25]. We evaluated the
1145 HyDrop v2 and 10x mouse motor cortex models by taking their predictions for these regions and
1146 calculating specificity through the *crested.pp._utils._calc_proportion* function. The specificity
1147 scores per model were then used to assess precision and recall, as was done in previous work[12].
1148 Similarly, from the scATAC-seq peak heights, we calculated specificity scores to obtain precision
1149 and recall scores. Ground truth labels were obtained from the annotation of the validated
1150 enhancers.

As the 10x dataset had three cell types not found in the HyDrop dataset (SstChodl, Sncg, and VLMC), we merged them into the Sst, Vip and Endo classes respectively by taking the max prediction and peak heights between the merged classes. The HyDrop v2 dataset on the other hand has a L4IT class not present in the 10x data, which is why it was merged with the L5IT class also based on maximal prediction and peak height between the two classes.

Fly

Samples generated with the HyDrop v2 platform and 10x v2 were extracted from the count matrix generated for the integrated samples into two count matrixes. Again, using pycisTopic[5], LDA was performed with 220 topics for HyDrop v2 and 200 topics for 10x v2. For downstream training of sequence models per sequencing technique, pseudobulk profiles were generated in pycisTopic[5] with MACS2 peak calling based on grouping cells in previously annotated cell types from the full data set excluding unannotated clusters.

The S2F model was trained with the CREsted package following a version of the default peak regression parameters adapted for fly. Briefly, the data was divided into train, validation and test sets. The regions in chromosome 2R were evenly divided into two to use as validation and test sets and the remaining chromosomes were used as the training set. The original region length of 500bp was kept. Peak heights were normalized per chromosome to a target mean accessibility of 0.5. After normalization, z-scores of peak heights were calculated per region. For each cell type, top 3000 regions with the highest z-scores were kept and the accessibility values of all the other regions were set to zero for that cell type. CosineMSELoss (from crested.tl.losses) was used along with the default optimizer and metrics from default CREsted peak regression configuration. The *deeptopic_cnn* model architecture was used with the following optional parameters: *filters=500, conv_do=0.5.* Since the default *deeptopic_cnn* model architecture has an output activation that's incompatible with regression task, it was replaced with a *softplus* activation. Two forms of augmentations were used: Before training, the training data was augmented using reverse complementation, this is achieved by adding the reverse complement of each sequence to the training data keeping the same target vector as the original sequence. During the training, each input region was stochastically shifted up to 3bp on either direction, still keeping the original target vector.

We identified the top 2,000 highest predicted regions per cell type per model and calculated the contribution scores of regions that are in the intersection of HyDrop v2 and 10x v2 data sets for the respective cell type. Later, these input sequences and contribution scores were used as input to *tfmodisco lite*-software (RRID:SCR_024811), using the available wrappers in CREsted package to find the most important patterns identified by 10x and HyDrop v2 models

per cell type. An importance threshold of 5 was handled to select the most important motifs displayed

10-fold cross-validation and selection of 500 bp regions in 2kb window

To evaluate the ability of our S2F models to capture biologically relevant information, we made use of validated enhancers downloaded from https://enhancers.starklab.org/ and lifted over to dm6 genome annotation with UCSC. The original cell type annotations were manually translated into the cell types used in this paper (Table S2). Each ~2kb enhancer region (merged for the annotated cell types) was scanned with a sliding window approach of 500 bp windows in steps of 10bp over the whole enhancer with the 10-fold cross-validated models. Then, the 500bp regions showing the highest CREsted predicted accessibility for all matching annotated cell types were selected based on the highest correlations between predicted and ground truth insertions.

sciATAC-seq based models

The trained models were obtained from https://doi.org/10.5281/zenodo.8011697. The enhancer activity models for used for all the analysis. The 501bp synthetic DNA sequences were acquired from Almedia et al.[15]. The sequences were flanked on each side by 250bp random sequences to acquire a 1001bp sequence. The nucleotide contribution scores were calculated for one replicate model for each of the ten cross-validation folds, from the relevant tissue (except for the epidermis, where none of the provided replicates of fold 5 were working). The final contribution score was calculated by averaging all the contribution scores per sequence. The visualization of the contribution scores was done in CREsted software.

Footprinting with PRINT

Footprint scores calculations were carried out using the default PRINT v3 procedure as described in https://ruochiz.com/scprinter_doc/index.html (scPRINTER python implementation of PRINT, https://zenodo.org/records/13963610). For both, mouse and fly, we used the estimated Tn5 bias files provided by the original authors. As Tn5 insertion inputs, we used the Hydrop v2 and 10x v2 fragment files preprocessed by PUMATAC pipeline[19] for in-house generated data and cellranger-arc (10x Genomics) for public the mouse multiome cortex data[46]. The data was grouped based on the cell barcodes annotated as previously described.

For mouse, we inspected the footprints of validated enhancer regions from the BICCN challenge[12]. For fly, we calculated footprints for all Drosophila embryo enhancers[17] active in stages 15-16 downloaded from https://enhancers.starklab.org/ and lifted over to dm6 genome annotation with UCSC. Each ~2kb enhancer region was scanned with a sliding window approach of 500 bp windows in steps of 10bp over the whole enhancer. Then, the 500bp regions showing the highest CREsted predicted accessibility for all matching annotated cell types were selected

for further analysis based on the highest correlations between predicted and ground truth insertions.

Supplementary material

a

Bead production trials	%T	%C	Bead size relative to 10X Genomics v3.1 GEX beads	Bead stability post refrigeration at -80*C	Dissolution time (10 mM DTT) relative to 10X Genomics v3.1 GEX beads
1	8.5	4	1.65	Unstable	0.9
2	10	4	1.1	Stable	∞*
3	15	2	0.95	Stable	∞*
4	15	4	1.1	Stable	∞*
5	9	2	3.3	Stable	0.95
6	9	4	1.1	Stable	2.1
7	10	2	0.94	Stable	1.2

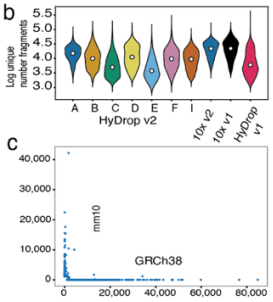

d

HyD ATAC bead batches	Acryd composition % T	% C	Acrydite primer Concentration	Microfluidics chip used	Flow Rate (monomer/oil)	Bead Size (um)	Additional Remarks
batch 1	0.085	0.04	4 uM	Atrandi MCN-G3	400/400	68	
batch 2	0.085	0.04	4 uM	Atrandi MCN-G4	300/1000	62.5	
batch 3	0.085	0.04	4 uM	inhouse chip 4 and 6	400/500	63	
batch 4	0.1	0.02	4 uM	inhouse chip 4 and 5	400/500	65.18	
batch 5	0.1	0.02	4 uM	inhouse chip 4 line 1 or 7	400/550	68.62	
batch 6	0.1	0.02	4 uM	inhouse chip 1 line 6	400/770	58.2	
batch 7	0.1	0.02	4 uM	inhouse chip 6 line 5	400/750	67.2	additional washes prior to mixing beads

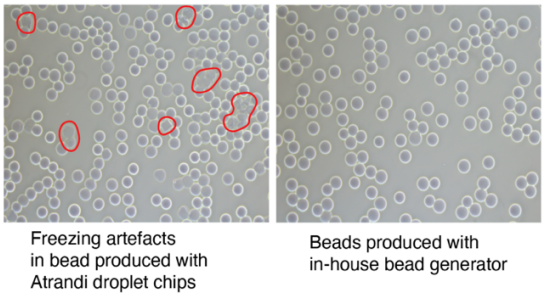

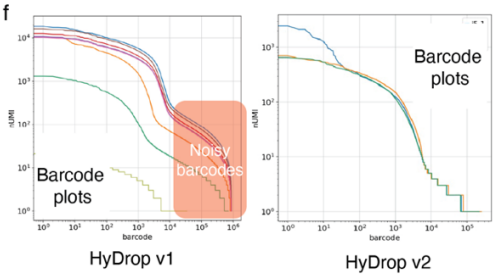

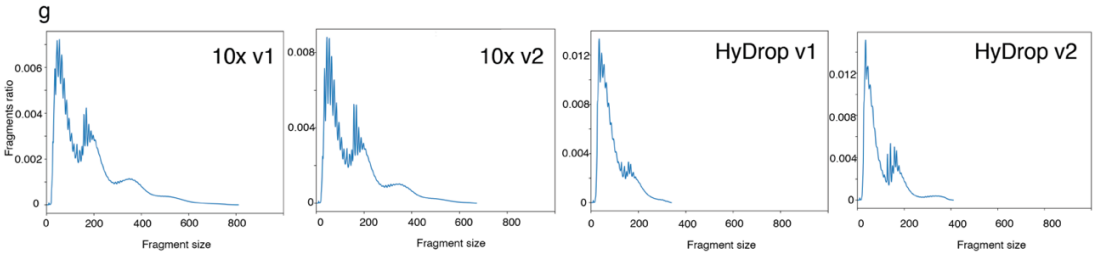

Fig S1|Improvement of HyDrop v2 bead generation. a, Characterization of bead quality and stability with different monomer compositions. Different percentages of total monomer and cross linker composition is varied during different bead productions and the stability of the beads are evaluated using three different characteristics: i.) bead size variations, ii.) bead stability post refrigeration, and iii.) dissolution time of the beads in a reducing environment relative to 10X genomics NextGEM 3' RNA beads. **b,** log-transformed number of unique fragments of experiments pooled for seven different bead batches of HyDrop v2 compared to pooled 10x v2, 10xv1, and HyDrop v1 samples. The median is shown as white dot. **c**, Barnyard of HyDrop v2 protocol with mouse and human cell line. **d.** Table illustrating different parameter and characteristics of different bead production batches. **e.** Bright field image of the beads showing freezing artifact in suboptimal bead batch productions. **f.** Barcode ranking plot showing noisy barcode contamination in the HyDrop v1 beads arising from the barcode bleeding during the production. **g**, Fragment size plot of 10x v1, 10x v2, HyDrop v1, and HyDrop v2 experiment. 10x data shown is downloaded from 10x Genomics website.

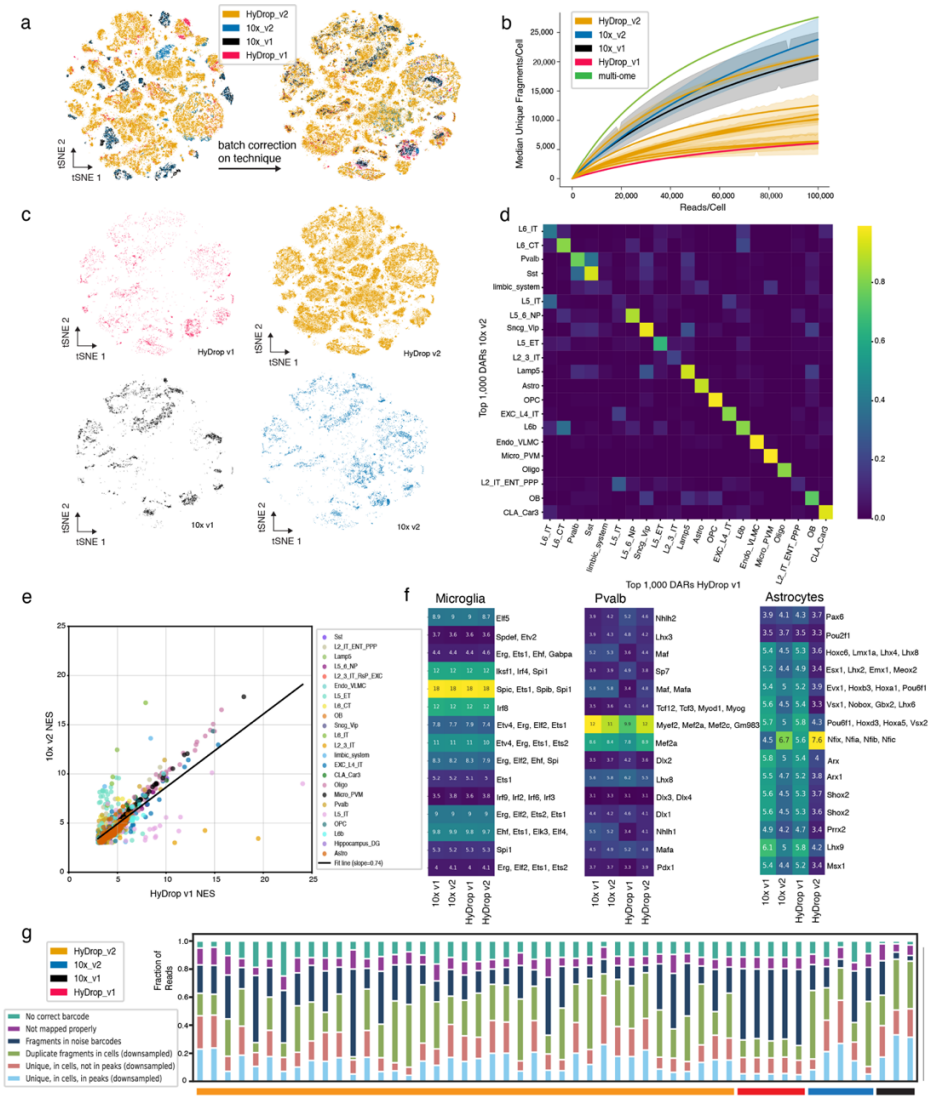

Fig. S2|Quality metrics across techniques in mouse cortex data. **a**, *t*-distributed stochastic neighbor embedding (tSNE) of all 141,010 cells across 44 experiments colored by technique used, left: no batch correction, right: batch corrected for the used technique. Data points were randomly shuffled before plotting. **b**, Sequencing efficiency compared across 10x v1 and v2, multi-ome (black), HyDrop v1 and HyDrop v2 beads (7 batches). The colors are shown in a. **c**, *t*-distributed stochastic neighbor embedding (tSNE) showing the distribution of cells in combined embedding in a, 2 experiments 10x v1 with a total of 10,177 cells, 2 experiments 10x v2 with a total of 13,123 cells, 5 experiments HyDrop v1 with a total of 7,163 cells, 35 experiments HyDrop v2 with a total of 110,547 cells). **d**, Heatmap for top 1000 DARs per cell type correlated between 10x v2 and HyDrop v1 data. **e**, Scatterplot of normalized enrichment score (NES) of cell-type-specific transcription motifs, dots represent a common motif between HyDrop v1 and 10x v2 data colored per cell type. **f**, NES of microglia, Pvalb, and astrocytes divided per technique. **g**, Stacked bar plot showing the fraction of reads across each step of data processing using the PUMATAC pipeline ('Unique, in cells, in peaks': final fraction of sequencing reads retained in count matrices). The colors at the bottom of the plot indicate the technique of the experiment. The data is down-sampled to 36kRPC.

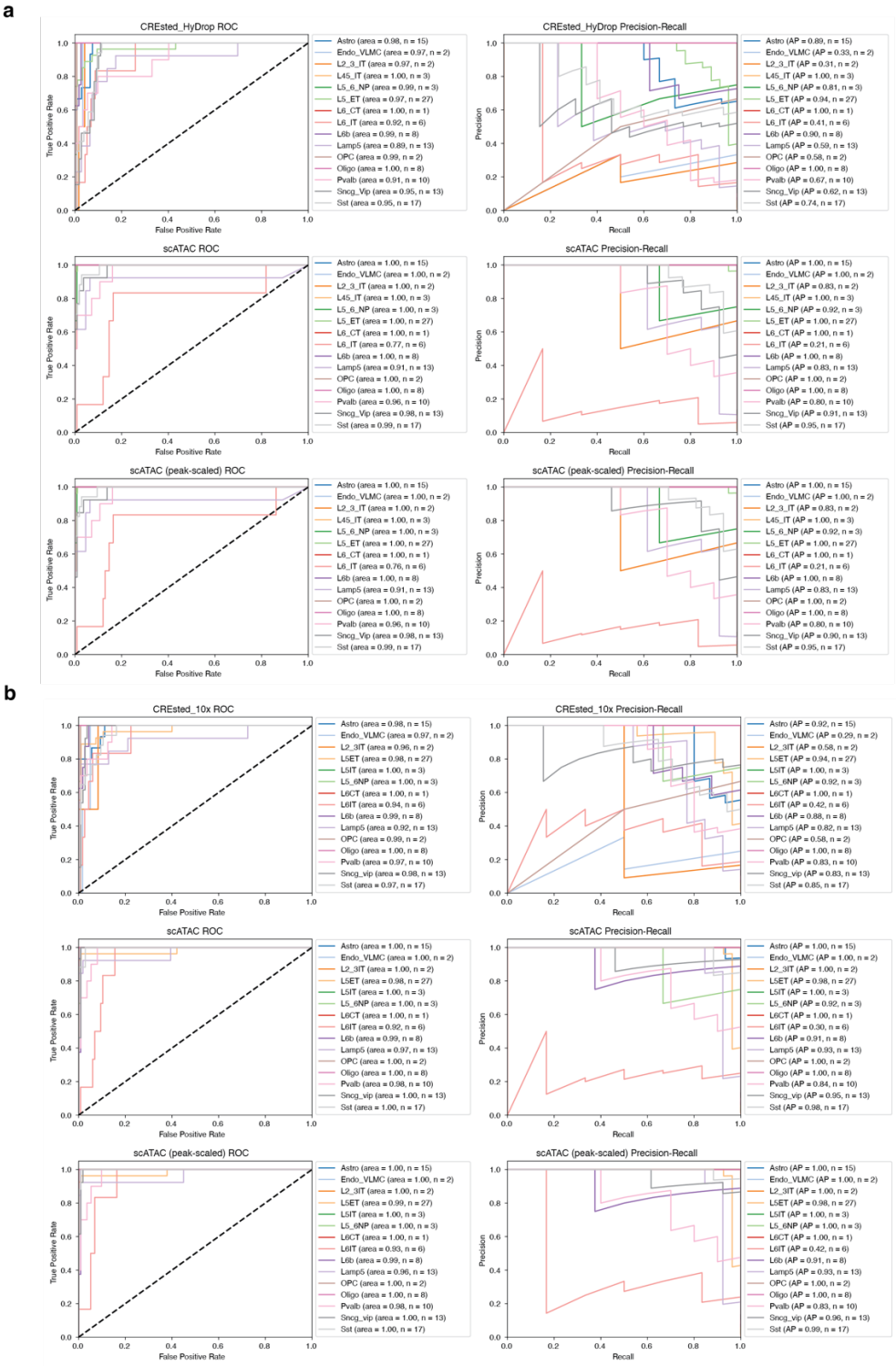

Figure S3. **Overview of prediction performance on *in vivo* validated mouse motor cortex enhancers per cell type** ROC and PR curves from specificity scores per cell type on *in vivo* validated of the Hydrop v2 CREsted model, HyDrop scATAC-seq data and peak-scaled HyDrop v2 scATAC-seq data (**a**), and of the 10x CREsted model, 10x scATAC-seq data and peak-scaled 10x scATAC-seq data (**b**).

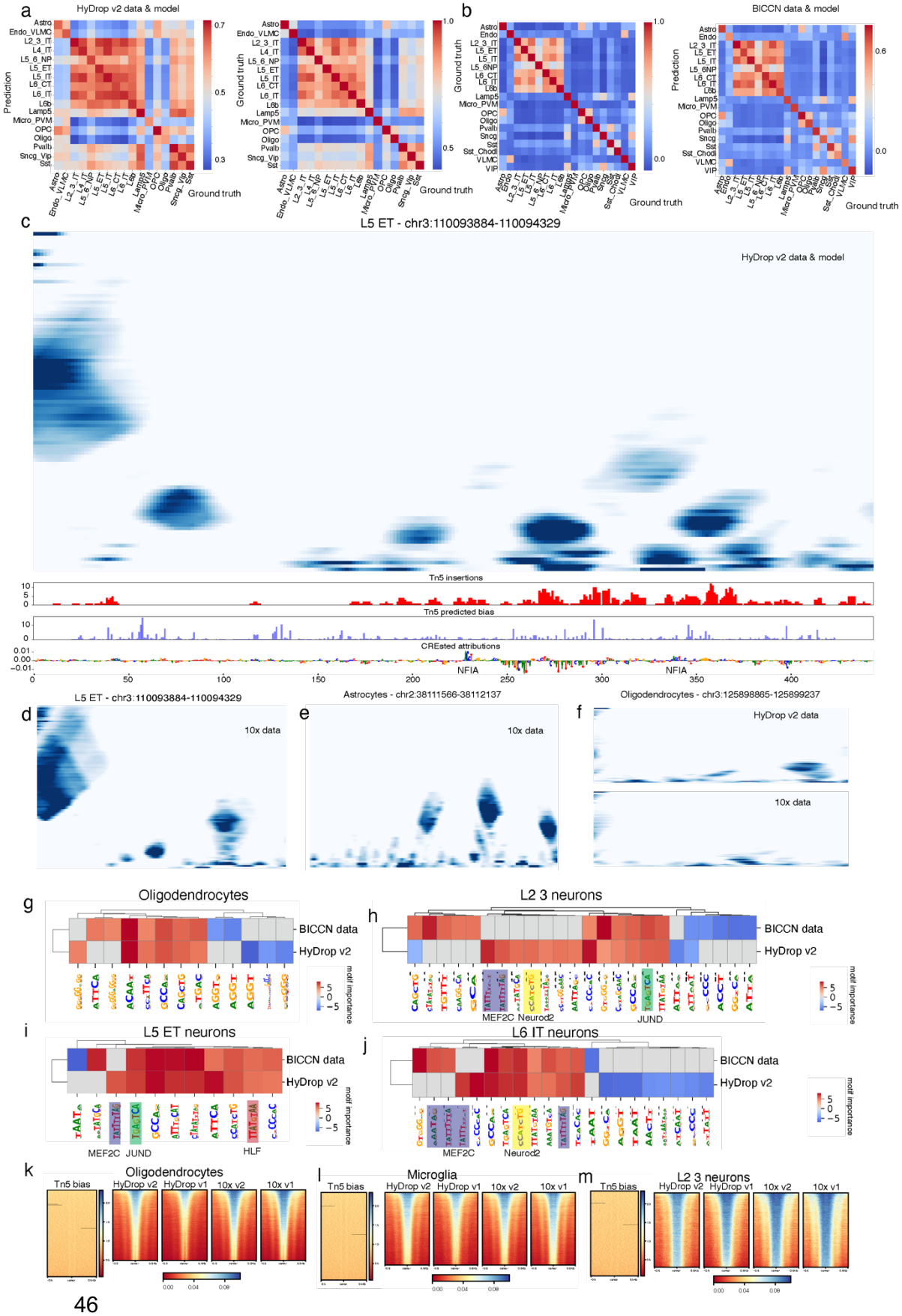
a
HyDrop v2 data & model
Prediction
Ground truth
b
BICCN data & model
c
L5 ET - chr3:110093884-110094329
HyDrop v2 data & model
Tn5 insertions
Tn5 predicted bias
CREsted attributions
NFIA
d
L5 ET - chr3:110093884-110094329
10x data
e
Astrocytes - chr2:38111566-38112137
10x data
f
Oligodendrocytes - chr3:125898865-125899237
HyDrop v2 data
10x data
g
Oligodendrocytes
BICCN data
HyDrop v2
motif importance
h
L2 3 neurons
MEF2C Neurod2
JUND
i
L5 ET neurons
MEF2C JUND
HLF
j
L6 IT neurons
MEF2C
Neurod2
k
Oligodendrocytes
Tn5 bias
HyDrop v2
HyDrop v1
10x v2
10x v1
l
Microglia
m
L2 3 neurons

1255

Fig. S4|Sequence model comparison and multiscale footprinting in mouse cortex. a, Heatmap of correlation of prediction by HyDrop v2 model with ground truth (left), self-correlation of HyDrop v2 data as ground truth (right) for HyDrop v2 data. **b**, Heatmap of correlation of prediction by 10x v2 model with ground truth (right), self-correlation of 10x v2 data as ground truth (left) for 10x v2 data. **c**, Multiscale footprint of the region (mm10 chr3:110093884-110094329) in L5 ET neurons from HyDrop v2 data. Bottom tracks show Tn5 insertion, the predicted Tn5 bias and the nucleotide contribution scores based on the HyDrop v2 sequence model. Previously described TF binding sites are highlighted for the corresponding TF. **d**, Multiscale footprint of the region (mm10 chr3:110093884-110094329) in L5 ET neurons from 10x data. **e,** Multiscale footprint of the region (mm10 chr3:110093884-110094329) in astrocytes from 10x data (HyDrop v2 shown in Figure 3j. **f**, Multiscale footprint of the region (mm10 chr3:125898865-125899237) in oligodendrocytes from HyDrop v2 data (top) and 10x data (bottom) **e**, Multiscale footprint of the regions shown in c (upper) and d (bottom) in BICCN (10x multi-ome data). **g-j**, Evaluation of motif importance scores (threshold set on 4.25) overlapping regions (present in HyDrop v2 and 10x data) for cell type identity indicated by the BICCN (10x) data-based model and HyDrp v2 data-based model for oligodendrocytes (**g**), L2 3 (**h**), L5 ET (**i**), and L6 IT neurons (**j**), **k-m**, Mouse-specific Tn5 bias from Hu et al., (2025) plotted on cell type-specific DARs and carrot plot showing the regions of accessible chromatin ±0.5 kb around the center of DARs sorted by the highest (blue) to lowest (red) accessibility in for HyDrop v2, HyDrop v1, 10x v2, and 10x v1 data for oligodendrocytes (**k**), microglia (**l**), and L2 3 neurons (**m**).

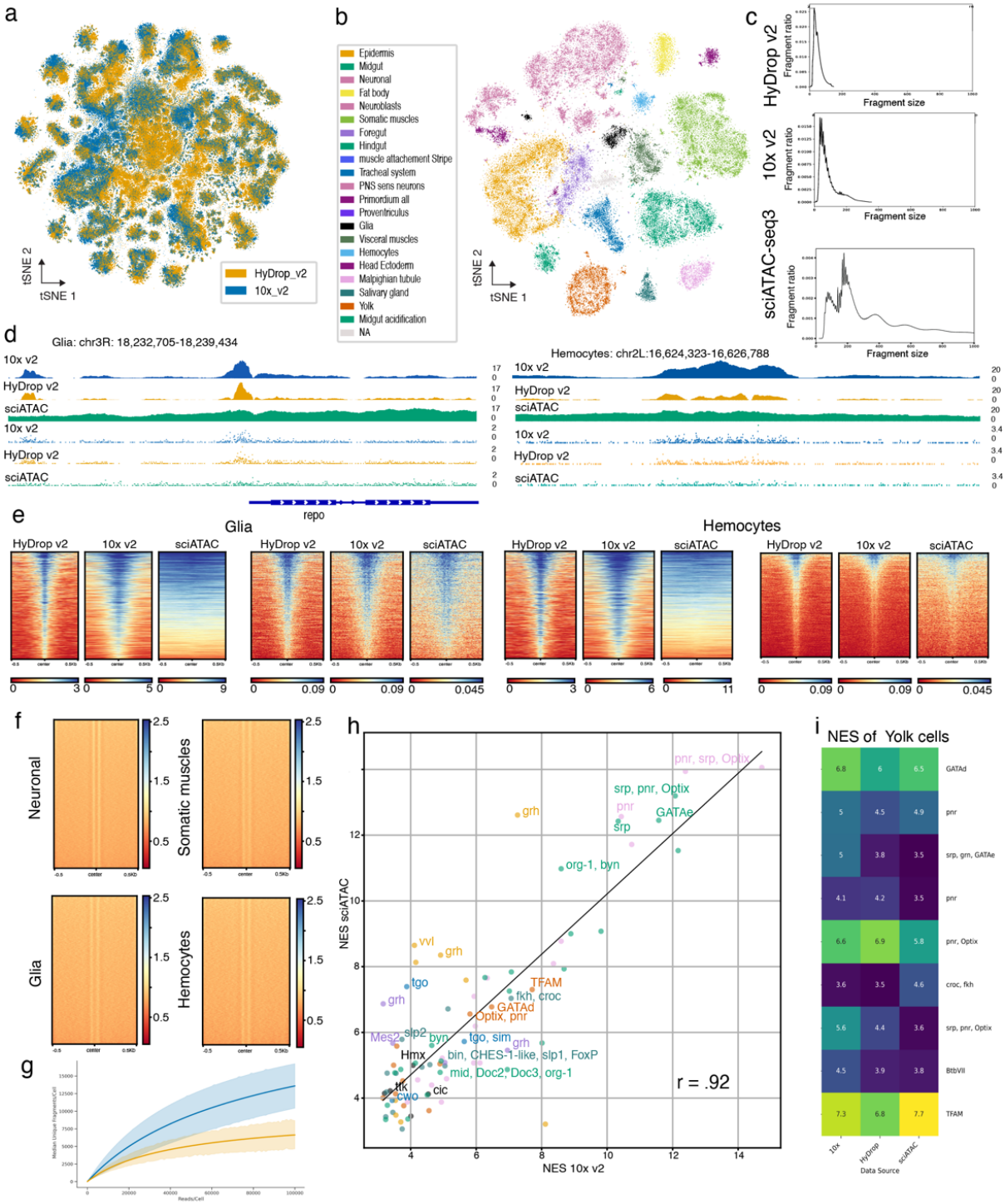

Fig. S5|HyDrop v2 captures cellular diversity comparable to 10x and more accurate than sciATAC in developing Drosophila melanogaster. **a,** *t*-distributed stochastic neighbor embedding (tSNE) of all 607,330 cells generated with HyDrop v2 (340,604, 18 experiments) and 10x v2 (266,736 cells, 5 experiments) colored by technique, batch correction according to wet lab protocol used to generate data. Data points were randomly shuffled before plotting. **b,** *t*-distributed stochastic neighbor embedding (tSNE) of 61,480 cells of 16-20h AEL extracted from sciATAC embryo atlas (Calderon

et al., 2022) colored by cell type. Data points were randomly shuffled before plotting. **c,** Fragment size plot of HyDrop v2, 10x v2 and sciATAC-seq3 experiments. d, Genome tracks of cell-type specific DARs down sampled to the smallest count present for each technique, 1,247 cells in glia and 1,002 cells in hemocytes. The shown genome tracks are normalized for the fragment count. **d,** Carrot plot showing the regions of accessible chromatin ±0.5 kb around the center of DARs sorted by the highest (blue) to lowest (red) accessibility for glia and hemocytes for HyDrop v2, 10x v2, and sciATAC data. Per cell type, the left plots are generated using the coverage while the right plots are generated using the cut site information extracted from cell-type specific fragment files. **e,** Drosophila-specific Tn5 bias from Hu et al., (2025) plotted on DARs of neuronal cells, somatic muscle cells, glia, and hemocytes. **f,** Sequencing efficiency compared between HyDrop v2 and 10x v2 samples. The colors are shown in a, the labels are shown for the top three motifs per cell type. **g,** Scatterplot of normalized enrichment score of cell-type-specific transcription motifs, dots represent a common motif between sciATAC and 10x v2 data colored per cell type as shown in b. h, Heatmap for top 1000 DARs Yolk cells of 10x v2, HyDrop v2, and sciATAC data. DAR: differentially accessible region.

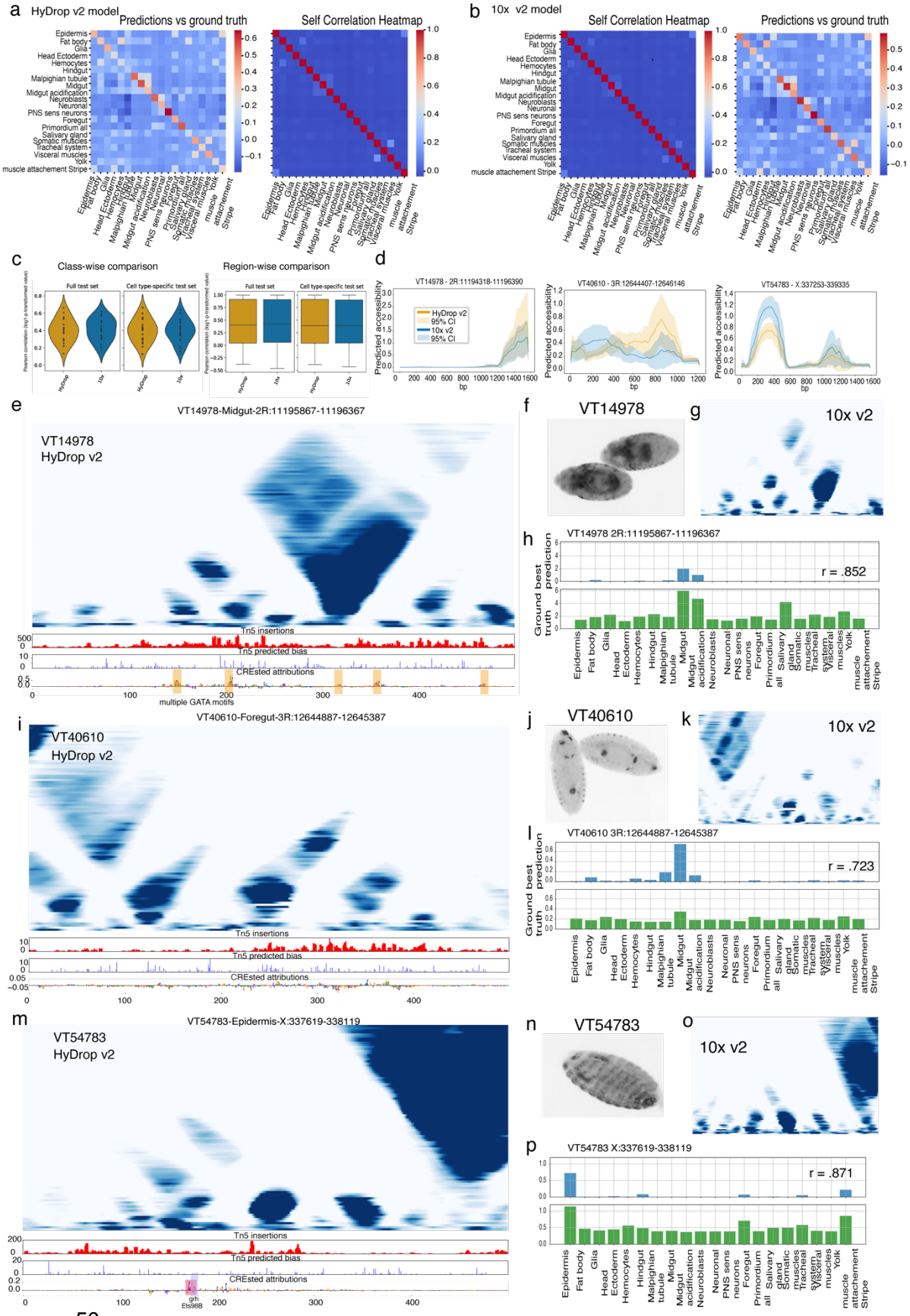
a
HyDrop v2 model
Predictions vs ground truth
Self Correlation Heatmap
b
10x v2 model
Self Correlation Heatmap
Predictions vs ground truth
c
Class-wise comparison
Region-wise comparison
Full test set
Cell type-specific test set
d
VT14978 - 2R:11194318-11196390
VT40610 - 3R:12644407-12646146
VT54783 - X:337253-339335
HyDrop v2
95% CI
10x v2
95% CI
Predicted accessibility
bp
e
VT14978-Midgut-2R:11195867-11196367
VT14978
HyDrop v2
Tn5 insertions
Tn5 predicted bias
CREsted attributions
multiple GATA motifs
f
VT14978
g
10x v2
h
VT14978 2R:11195867-11196367
r = .852
Ground best truth
prediction
i
VT40610-Foregut-3R:12644887-12645387
VT40610
HyDrop v2
Tn5 insertions
Tn5 predicted bias
CREsted attributions
j
VT40610
k
10x v2
l
VT40610 3R:12644887-12645387
r = .723
m
VT54783-Epidermis-X:337619-338119
VT54783
HyDrop v2
Tn5 insertions
Tn5 predicted bias
CREsted attributions
grh
Ets98B
n
VT54783
o
10x v2
p
VT54783 X:337619-338119
r = .871
Epidermis
Fat body
Glia
Head Ectoderm
Hemocytes
Hindgut
Malpighian tubule
Midgut
Midgut acidification
Neuroblasts
Neuronal
PNS sens neurons
Foregut
Primordium all
Salivary gland
Somatic muscles
Tracheal system
Visceral muscles
Yolk
muscle attachement Stripe

Fig. S6|HyDrop v2 sequence model matches results of 10x v2 sequence model and footprinting. a, Heatmap of correlation of prediction by HyDrop v2 model with ground truth (left), self-correlation of HyDrop v2 data as ground truth (right) for HyDrop v2 data. **b**, Heatmap of correlation of prediction by 10x v2 model with ground truth (right), self-correlation of 10x v2 data as ground truth (left) for 10x v2 data. **c**, Model comparison of sequence models trained on HyDrop v2 data (orange) and the 10x v2 data set (blue). The accuracy of the predictions evaluated based on the ground truth of region accessibility is compared on class-wise (top) and region-wise level (bottom) for both the full test set in the data and cell type-specific test sets. **d**, Predicted accessibility of 500 bp windows of VT3067 enhancer from VDRC library. Both, the predictions based on the HyDrop v2 and 10x v2 data are shown confidence intervals reflect 10-fold cross-validation models. **e**, Multiscale footprint of 500bp region in VT14978 in midgut cells from HyDrop v2 data only. The bottom track shows Tn5 insertion, the predicted Tn5 bias, and the nucleotide contribution scores based on the HyDrop v2 sequence model. Previously described TF binding sites are highlighted for the corresponding TF. **f,** *In situ* hybridization of VT14978-Gal4 reporter embryos stage 15 with antisense Gal4 probe by Kvon et al. (2014). **g**, Multiscale footprint of 500bp region in VT14978 in midgut cells from 10x v2 data. **h**, Prediction (top) versus ground truth (bottom) of 500bp region within 2kb long VDRC enhancer VT14978 active in midgut cluster. **i**, Multiscale footprint of 500bp region in VT40610 in foregut cells from HyDrop v2 data only. The bottom track shows Tn5 insertion, the predicted Tn5 bias, and the nucleotide contribution scores based on the HyDrop v2 sequence model. Previously described TF binding sites are highlighted for the corresponding TF. **j,** *In situ* hybridization of VT40610-Gal4 reporter embryos stage 15 with antisense Gal4 probe by Kvon et al. (2014). **k**, Multiscale footprint of 500bp region in VT40610 in foregut cells from 10x v2 data. **l**, Prediction (top) versus ground truth (bottom) of 500bp region within 2kb long VDRC enhancer VT40610 active in midgut cluster. **m**, Multiscale footprint of 500bp region in VT54783 in epidermis cells from HyDrop v2 data only. The bottom track shows Tn5 insertion, the predicted Tn5 bias, and the nucleotide contribution scores based on the HyDrop v2 sequence model. Previously described TF binding sites are highlighted for the corresponding TF. **j,** *In situ* hybridization of VT54783-Gal4 reporter embryos stage 15 with antisense Gal4 probe by Kvon et al. (2014). **k**, Multiscale footprint of 500bp region in VT54783 in epidermis cells from 10x v2 data. **l**, Prediction (top) versus ground truth (bottom) of 500bp region within 2kb long VDRC enhancer VT54783 active in midgut cluster. VDRC: Vienna Drosophila Resource Center

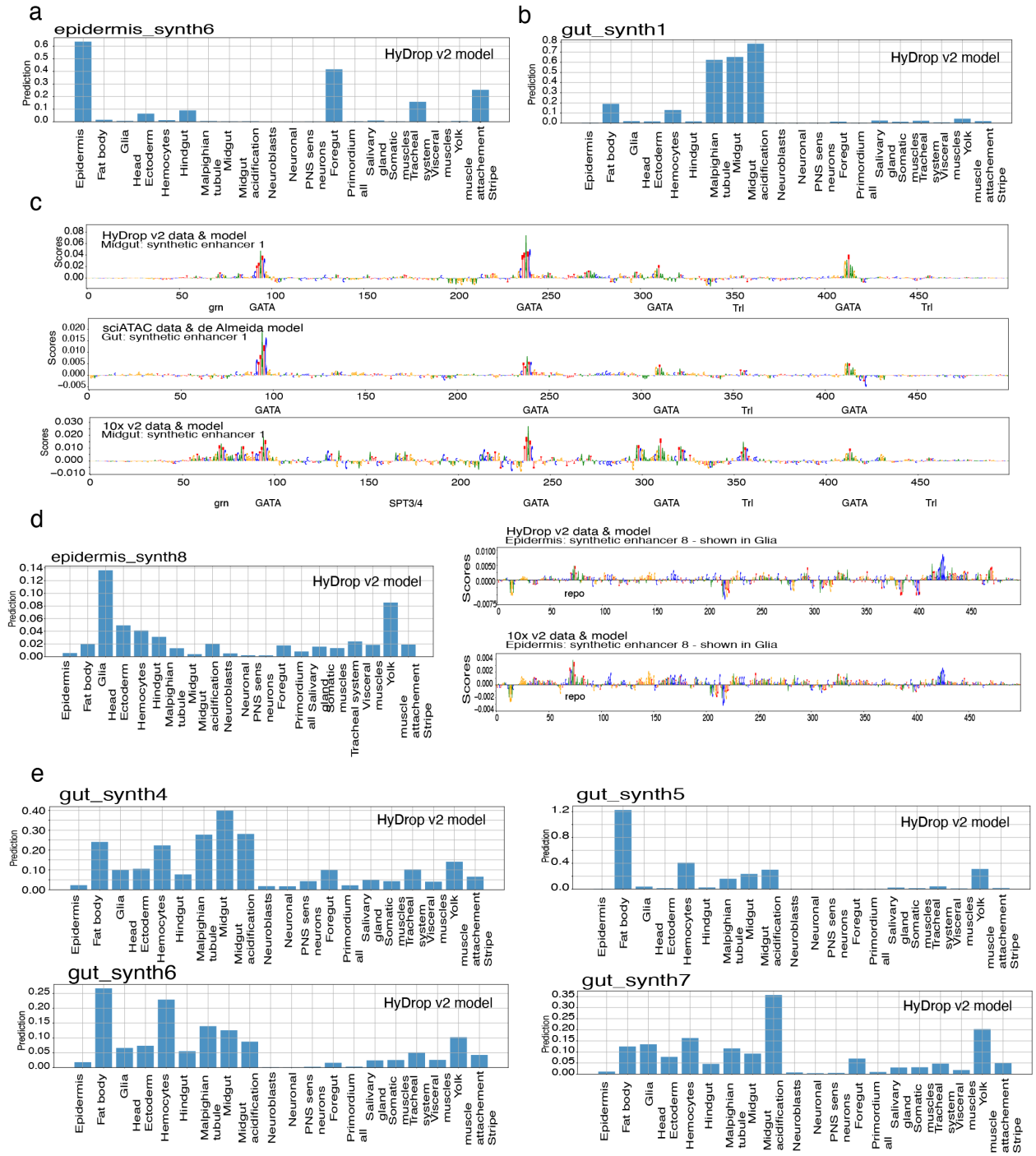

Fig. S7|Evaluation of synthetic enhancers designed by de Almeida et al (2023) by HyDrop v2 model. a, Prediction of tissue accessibility of synthetic enhancer designed for epidermis cells in 10-12h embryos. Enhancers were designed by de Almeida et al. (2023) and scored with the HyDrop v2 model. Accessibility is specifically predicted for epidermis cells in the HyDrop v2 data. **b**, Prediction of tissue accessibility of synthetic enhancer designed for gut cells in 10-12h embryos. Accessibility is specifically predicted for midgut cells in the HyDrop v2 data. **c**, Nucleotide contribution score of the 500 bp of synthetic enhancer designed to be active in gut cells based on sciATAC data by de Almeida et al. (2023): HyDrop v2 and 10x v2 model predictions shown for midgut cells versus predictions by the original model for

general gut cells. **d,** Prediction of tissue accessibility of synthetic enhancer designed for epidermis cells in 10-12h embryos. Accessibility is specifically predicted for glial cells in the HyDrop v2 data (left). Right: Nucleotide contribution score of the 500 bp of synthetic enhancer designed to be active in epidermis cells based on sciATAC data by de Almeida et al. (2023): HyDrop v2 and 10x v2 model predictions shown for glial cells instead showing a *repo* motif. **e**, Prediction of tissue accessibility of synthetic enhancer designed for gut cells in 10-12h embryos. Enhancers were designed by de Almeida et al. (2023) but did not give signal *in vivo*. Here, the synthetic sequences are scored with the HyDrop v2 model showing predicted accessibility in other tissues than the gut.

Table S1. Key resource table

RESOURCE TYPE	RESOURCE NAME	SOURCE	IDENTIFIER	NEW/REUSE	ADDITIONAL INFORMATION
Chemical, peptide, or recombinant protein	acrylamide	Merck	A4058	REUSE	
Chemical, peptide, or recombinant protein	N,N'-Bis(acryloyl)cystamine	Merck	A4929	REUSE	
Chemical, peptide, or recombinant protein	ammonium persulfate	Merck	9913	REUSE	
Chemical, peptide, or recombinant protein	HFE7500	fluorochem	F051243	REUSE	
Chemical, peptide, or recombinant protein	2 weight % 008- FluoroSurfactant in HFE7500	RAN Biotech	008-FluoroSurfactant-2wt	REUSE	
Chemical, peptide, or recombinant protein	mineral oil	Merck	M5904	REUSE	
Chemical, peptide, or recombinant protein	N,N,N',N'-Tetramethylethylenediamine	Merck	T7024	REUSE	
Chemical, peptide, or recombinant protein	1H,1H,2H,2H-Perfluoro-1-octanol	Merck	370533	REUSE	
Chemical, peptide, or recombinant protein	SPAN-80	Merck	S6760	REUSE	
Chemical, peptide, or recombinant protein	hexane	Acros	364370010	REUSE	
Chemical, peptide, or recombinant protein	Triton X-100	merck	X100	REUSE	
Chemical, peptide, or recombinant protein	Tween-20	merck	P1379-100	REUSE	
Chemical, peptide, or recombinant protein	ATP	New England Biolabs	P0756	REUSE	
Chemical, peptide, or recombinant protein	T4 ligase	New England Biolabs	M0202	REUSE	
Chemical, peptide, or recombinant protein	BSA 30%	Merck	A8577	REUSE	
Chemical, peptide, or recombinant protein	Digitonin	Promega	G944A	REUSE	
Chemical, peptide, or recombinant protein	Tris-HCl pH 7.5, 1M	Invitrogen	15567-027	REUSE	
Chemical, peptide, or recombinant protein	Tris-HCl pH 8, 1M	Invitrogen	15568-025	REUSE	
Chemical, peptide, or recombinant protein	MgCl2 1M	Invitrogen	AM9530	REUSE	
Chemical, peptide, or recombinant protein	NaCl 5M	Invitrogen	AM9759	REUSE	
Chemical, peptide, or recombinant protein	EDTA 0.5 M	Invitrogen	AM9261	REUSE	
Chemical, peptide, or recombinant protein	NaOH 10N	Alfa Aesar	J63736	REUSE	
Chemical, peptide, or recombinant protein	Brij-35	ThermoFisher	20150	REUSE	
Protocol	Microfluidic Chip Production v1.1 V.4	https://www.protocols.io/view/microfluidic-chip-production-v1-1-6qpvrdq7pgmk/v4	dx.doi.org/10.17504/protc	REUSE	
Protocol	HyDrop v2 Bead Generation & Ligation Barcoding	dx.doi.org/10.17504/protocols.io.8epv5n11dv1bb/v1	dx.doi.org/10.17504/protc	NEW	
Protocol	HyDrop-v2-ATAC	dx.doi.org/10.17504/protocols.io.x54v97mmpg3e/v1	dx.doi.org/10.17504/protc	NEW	
Critical commercial assay	10x Genomics scATAC v2	10x Genomics		REUSE	
Oligonucleotide	P7 indexing primer	IDT		REUSE	Standard desalted: CAAGCAGAAGACGGCATACGAGATXXXXXXXXXXGTCTCGTGGGCTCGGAGATGTG
Oligonucleotide	P5-Partial	IDT		REUSE	Standard desalted: AATGATACGGCGACCACCGA
Oligonucleotide	Bead handle	IDT		NEW	HPLC purified: /5Acryd/iThioMC6-D/AATGATACGGCGACCACCGAGATCTACAC
Experimental model: Drosophila lines	DGRP-639	Bloomington	RRID:BDSC_25199	REUSE	
Experimental model: Drosophila lines	DGRP-502	Bloomington	RRID:BDSC_28204	REUSE	
Experimental model: Drosophila lines	DGRP-409	Bloomington	RRID:BDSC_28278	REUSE	
Biological sample	Mouse cortex	female P57 with C57B/6J background		REUSE	
Experimental model: Cell line	mouse melanoma			REUSE	
Experimental model: Cell line	MCF-7		RRID:CVCL_0031	REUSE	
Software/code	CREated v. 1.3.0	https://pypi.org/project/created/	RRID:SCR_026617	REUSE	
Software/code	tfmodisco-lite v.2.2.1	https://pypi.org/project/modisco-lite/	RRID:SCR_024811	REUSE	
Software/code	pycistopc v2.0a0	https://pycistopic.readthedocs.io/en/polars/	RRID: SCR_026618	REUSE	
Software/code	PUMATAC v0.0.1	https://zenodo.org/records/7924251	RRID:SCR_026624	REUSE	
Software/code	Nextflow v21.04.3		RRID:SCR_024135	REUSE	
Software/code	Scrublet		RRID:SCR_018098	REUSE	
Software/code	pyCisTarget v1.0a2	https://pycistarget.readthedocs.io/en/latest/	RRID:SCR_026626	REUSE	
Software/code	scATAC-seq Fragment Tools	https://aertslab.github.io/scatac_fragment_tools/	RRID:SCR_026643	REUSE	
Software/code	Integrative Genomics Viewer (IGV)	https://igv.org	RRID:SCR_011793	REUSE	
Software/code	DeepTools2 v3.5.3	https://deeptools.readthedocs.io/en/latest/	RRID:SCR_016366	REUSE	
Software/code	scPRINTER (python implementation of PRINT) v3	https://zenodo.org/records/13963610	RRID:SCR_026644	REUSE	
Software/code	Drosophila embryo model by de Almeida et al.	https://doi.org/10.5281/zenodo.8011697		REUSE	
Software/code	mouse motor cortex sequence to function model Aerts	https://www.biorxiv.org/content/10.1101/2024.08.21.609075v1		REUSE	
Software/code	Keras v.3.0	https://keras.io/	RRID:SCR_026159	REUSE	
Software/code	TensorFlow v.2.19.0	https://www.tensorflow.org/	RRID:SCR_016345	REUSE	
Software/code	PyTorch v.2.6.0	https://pytorch.org/	RRID:SCR_018536	REUSE	
Dataset	Human genome (hg38)	https://hgdownload.cse.ucsc.edu/goldenPath/hg38/bigZips/		REUSE	
Dataset	Mouse genome (mm10)	https://hgdownload.cse.ucsc.edu/goldenPath/mm10/bigZips/		REUSE	
Dataset	Drosophila genome (dm6)	https://hgdownload.cse.ucsc.edu/goldenPath/dm6/bigZips/		REUSE	
Dataset	mouse motor cortex adata	https://www.biorxiv.org/content/10.1101/2024.08.21.609075v1		REUSE	
Dataset	Drosophila embryo atlas 16-20h development	https://www.science.org/doi/full/10.1126/science.abn5800		REUSE	
Dataset	list of tested mouse cortex enhancers	https://www.ncbi.nlm.nih.gov/pmc/articles/PMC11195086/		REUSE	
Other	images of VT VDRC fly lines embryo staining	https://enhancers.starklab.org/about		REUSE	

1340 **Table S2. VTID enhancers stage 15 and 16 by Kvon et al. (2014) annotated according to**

1341 **HyDrop Drosophila annotation**

VTID	Dm6 Chromo	Dm6 Start	Dm6 End	stg15_16	HyDrop_cell_types
VT1083	chr2L	2163674	2165773	antenno-maxillary-labial_complex;3|brain_subset;3	Neuronal
VT11145	chr2L	21843469	21845803	head_subset;3|dorsal_vessel;3|midgut_chamber;3	Midgut, Head_Ectoderm, Midgut_acidification
VT14335	chr2R	9930287	9932397	NA	NA
VT14616	chr2R	10459397	10461789	hindgut;5|anal_pad;4|atrium;4	Hindgut
VT14978	chr2R	11194318	11196390	amnioserosa;5|midgut_broad;3|ubiquitous;3	Midgut
VT15726	chr2R	12593526	12595724	head_subset;3|head_epidermis_broad;3|pharynx;3|trunk_ep	Epidermis, Head_Ectoderm, Foregut, Hindgut
VT1597	chr2L	3113886	3116075	salivary_gland;5|gonad;2	Salivary_gland
VT16530	chr2R	14173216	14175346	ubiquitous;4	NA
VT16613	chr2R	14334875	14336968	antenno-maxillary-labial_complex;3|amnioserosa;5	NA
VT17409	chr2R	15897411	15899572	ventral_nerve_cord_subset;4|anal_pad;3|brain_subset;4|mai	Neuronal, Malpighian_tubule, Head_Ectoderm
VT17873	chr2R	16783707	16785865	yolk;4|hemocyte;3|macrophage;3	Yolk, Hemocytes
VT18684	chr2R	18338586	18340728	brain_broad;5|ventral_nerve_cord_broad;5	Neuronal, Head_Ectoderm
VT19073	chr2R	19107715	19109845	head_epidermis_broad;5|trunk_epidermis_broad;5	Epidermis
VT19429	chr2R	19819410	19821552	tracheal_system_subset;3|anterior_spiracle;3	Tracheal_system
VT19535	chr2R	20026362	20028504	head_subset;3|anal_pad;5	Neuronal, Head_Ectoderm
VT19841	chr2R	20597698	20599839	head_subset;2	Neuronal, Head_Ectoderm
VT21015	chr2R	22802043	22803585	NA	NA
VT21151	chr2R	23049881	23051973	NA	NA
VT21433	chr2R	23592106	23594358	foregut;3	Proventriculus
VT21819	chr2R	24327840	24330065	head_subset;4|midgut_broad;3|head_epidermis_subset;5|tr	Neuronal, Midgut, Epidermis, Midgut_acidification
VT22068	chr2R	24807620	24809727	NA	NA
VT22223	chr2R	25106786	25108894	telson_subset;4|head_epidermis_ventral_broad;3	Epidermis, Head_Ectoderm
VT23462	chr3L	373888	375960	head_subset;4|salivary_gland_common_duct;4	Neural, Salivary_gland
VT23835	chr3L	1095173	1097593	lateral_epidermis_subset;3|ventral_midline;3|midgut_broad;:	Epidermis, Midgut, Midgut_acidification
VT23951	chr3L	1322658	1324778	trunk_epidermis_broad;3	Epidermis
VT26739	chr3L	6806613	6808816	trunk_epidermis_broad;5	Epidermis
VT28557	chr3L	10351940	10354125	head_subset;4|somatic_muscle;5	Neural, Somatic_muscles, Head_Ectoderm
VT29804	chr3L	12693742	12696663	midgut_chamber;2|proventriculus;4	Midgut, Proventriculus
VT3067	chr2L	6073895	6076535	midgut_broad;2|ventral_nerve_cord_broad;4|trunk_epiderm	Midgut, Neuronal, Head_Ectoderm, Midgut_acidification, Neuroblasts
VT31409	chr3L	15763704	15765967	antenno-maxillary-labial_complex;3|telson_subset;3|midgut	Midgut, Midgut_acidification
VT31552	chr3L	16043310	16045539	brain_broad;2	Neuronal, Neuroblasts
VT32972	chr3L	18787471	18789555	salivary_gland;5|fat_body;2	Salivary_gland, Fat_body
VT36347	chr3R	4451213	4453364	midgut_broad;3|ubiquitous;5|head_epidermis_subset;5|tru	Midgut, Epidermis, Head_Ectoderm, Midgut_acidification
VT38601	chr3R	8787084	8789298	head_subset;4|lateral_epidermis_subset;3|ventral_epidermis	Epidermis, Head_Ectoderm
VT39498	chr3R	10513249	10515382	head_subset;2|amnioserosa;4|midgut_chamber;4	Midgut
VT39530	chr3R	10569672	10571928	brain_broad;4|ventral_nerve_cord_broad;4	Neuronal, Neuroblasts
VT40599	chr3R	12621701	12623889	salivary_gland;5	Salivary_gland
VT40610	chr3R	12644407	12646146	pharynx;4|proventriculus;5|anterior_hindgut;5|esophagus;4	Foregut, Hindgut, Proventriculus
VT40611	chr3R	12645563	12648106	midgut_chamber;2	Midgut, Midgut_acidification
VT40612	chr3R	12648083	12650858	head_subset;3	Neuronal, Neuroblasts
VT41025	chr3R	13428001	13428951	NA	NA
VT41037	chr3R	13448589	13450735	visceral_muscle_broad;4	Visceral_muscles
VT42009	chr3R	15307864	15310235	somatic_muscle;5	Somatic_muscles
VT42358	chr3R	16005428	16007531	midgut_broad;2|proventriculus;4|salivary_gland;4|malpighia	Midgut, Salivary_gland, Malpghian_tubule, Proventriculus
VT4243	chr2L	8421920	8424099	antenno-maxillary-labial_complex;5|ventral_nerve_cord_sub	Neuronal, Neuroblasts, Hemocytes
VT42746	chr3R	16699060	16701215	salivary_gland;5|outer_optic_lobe;1	Salivary_gland, Neuronal
VT42747	chr3R	16700797	16702888	head_subset;3	Neuronal
VT42831	chr3R	16890314	16892448	ventral_nerve_cord_subset;3|brain_subset;3|dorsal_epiderm	Neuronal, Neuroblasts, Epidermis
VT42855	chr3R	16936443	16938643	head_subset;3|lateral_epidermis_subset;3|telson_subset;3|h	Epidermis, Neuronal, Neuroblasts
VT42863	chr3R	16950676	16952842	pharynx;3|trunk_epidermis_subset;3	Foregut, Epidermis
VT4320	chr2L	8578321	8580523	ventral_epidermis_subset;3|trunk_epidermis_subset;1|dorsa	Epidermis, Head_Ectoderm
VT43781	chr3R	18695700	18697823	pharynx;5|atrium;3	Foregut
VT44101	chr3R	19300581	19302962	pharynx;2|telson_subset;2|proventriculus;5	Foregut, Midgut
VT44107	chr3R	19314425	19316666	ventral_epidermis_subset;2|brain_subset;3	Neuronal, Neuroblasts, Head_Ectoderm
VT4448	chr2L	8841573	8843738	ventral_midline;2|brain_subset;3	Neuronal
VT45611	chr3R	22168686	22170923	head_subset;3|lateral_epidermis_subset;3|telson_broad;5	Epidermis
VT45651	chr3R	22253586	22255816	head_subset;5|stomatogastric_nervous_system;5	PNS_sens_neurons
VT47167	chr3R	25171908	25174205	NA	NA
VT47408	chr3R	25632148	25634323	brain_subset;2	Neuronal
VT47619	chr3R	26026378	26028970	head_subset;2|hypopharynx;3	Neuronal, PNS_sens_neurons
VT47640	chr3R	26064120	26066252	salivary_gland;5	Salivary_gland
VT48943	chr3R	28588434	28590577	midgut_chamber;2|brain_broad;1|hindgut;2|ventral_nerve_c	Midgut, Neuronal, Head_Ectoderm, Migut_acidification
VT48946	chr3R	28592856	28595111	brain_subset;1	Neuronal
VT49445	chr3R	29562062	29564342	lateral_epidermis_subset;5	Epidermis
VT49668	chr3R	29983451	29986358	head_epidermis_broad;5|pharynx;5|trunk_epidermis_broad;	Epidermis, Foregut, Head_Ectoderm
VT50195	chr3R	30923617	30925849	head_subset;3|midgut_chamber;4|midgut_interstitial_cell;4	Midgut
VT54783	chrX	337253	339335	ventral_epidermis_subset;3|salivary_gland;5|head_epidermis	Epidermis, Salivary_gland
VT55906	chrX	2651914	2654026	head_epidermis_broad;5|pharynx;4|trunk_epidermis_broad;	Foregut, Epidermis
VT57083	chrX	5054760	5056847	head_epidermis_broad;5|trunk_epidermis_broad;5|ubiquito	Epidermis
VT58723	chrX	8354492	8356703	antenno-maxillary-labial_complex;5|lateral_epidermis_subse	Epidermis
VT58999	chrX	8882617	8884691	antenno-maxillary-labial_complex;3|pharynx;5|proventriculu	Midgut, Foregut, Proventriculus
VT59092	chrX	9059967	9062117	midgut_chamber;5|head_epidermis_subset;4|trunk_epiderm	Midgut, Epidermis, Migut_acidification, Head_Ectoderm
VT62606	chrX	16169462	16171589	visceral_muscle_broad;5	Visceral_muscles
VT6436	chr2L	12589222	12591343	amnioserosa;3|midgut_broad;5|salivary_gland;4	Midgut, Salivary_gland, Head_Ectoderm
VT64887	chrX	20651972	20654082	ventral_nerve_cord_subset;1|brain_subset;1	Neuronal, Neuroblasts
VT7402	chr2L	14485084	14487223	head_epidermis_lateral_subset;2	Epidermis
VT7922	chr2L	15480181	15482932	NA	NA
VT8346	chr2L	16317691	16319794	posterior_hindgut;3|proventriculus;3|salivary_gland;5	Hindgut, Proventriculus, Salivary_gland
VT9081	chr2L	17748587	17750842	NA	NA
VT9675	chr2L	18890105	18892283	ventral_nerve_cord_subset;2|amnioserosa;4|brain_subset;2	Neuronal, Neuroblasts, Epidermis

1342